

## Original Article

**Cite this article:** Yang Y-L, Chen C-H, Qin S-P, Tang Y, Guo W-Q, and Qin Z-P (2023) Mineral textures, mineral chemistry and S isotopes of sulphides from the Tianbaoshan Pb–Zn–Cu deposit in the Sichuan–Yunnan–Guizhou triangle: implications for mineralization process. *Geological Magazine* **160**: 471–489. <https://doi.org/10.1017/S0016756822001054>

Received: 10 November 2021

Revised: 10 September 2022

Accepted: 14 September 2022

First published online: 19 December 2022

**Keywords:**


mineral textures; trace elements in sulphides; sulphur isotopes; fluids mixing; Tianbaoshan Pb–Zn deposit; Sichuan–Yunnan–Guizhou triangle

**Author for correspondence:**

Cui-Hua Chen,

Email: [chencuihua@cdut.edu.cn](mailto:chencuihua@cdut.edu.cn)

# Mineral textures, mineral chemistry and S isotopes of sulphides from the Tianbaoshan Pb–Zn–Cu deposit in the Sichuan–Yunnan–Guizhou triangle: implications for mineralization process

Yu-Long Yang<sup>1</sup> , Cui-Hua Chen<sup>1</sup>, Shun-Ping Qin<sup>2</sup>, Yao Tang<sup>1</sup>, Wen-Qi Guo<sup>1</sup> and Zhi-Peng Qin<sup>1</sup>

<sup>1</sup>College of Earth Sciences, Chengdu University of Technology, Chengdu, 610059, Sichuan, China and <sup>2</sup>Sichuan Huili Zinc & Plumbum Company Limited, Huili County, 615105, Sichuan, China

**Abstract**

The carbonate-hosted Pb–Zn deposits in the Sichuan–Yunnan–Guizhou (SYG) triangle region are important Indosinian deposits in South China. The Tianbaoshan deposit is a typical large Pb–Zn deposit in the SYG area and occurs as pipe-like type, hosted by Sinian dolostone. It contains ~26 Mt Zn–Pb ore (7.76–10.09 % Zn, 1.28–1.50 % Pb and 93.6 g t<sup>-1</sup> Ag) and >0.1 Mt Cu ore (2.55 % Cu). In this study, the detailed mineral textures, mineral chemical and sulphur isotopic compositions of the various sulphides have been analysed to constrain the abnormal enrichment mechanism and mineralization relationship. Four mineralization stages have been recognized: Stage 1, minor early pyrite (Py1) with relics and infill of intergranular dolomite or quartz grains; Stage 2, Cu mineralization with coarse-grained, elliptical crystal chalcopyrite (Cp1); (3) Stage 3, Zn mineralization with dark fine-grained sphalerite (Sph1) and light coarse-grained sphalerite (Sph2); and (4) Stage 4, as represented by a quartz–calcite assemblage with galena, minor pyrite (Py2) and chalcopyrite (Cp2). The petrography of the sulphide minerals (Py1, Cp1, Sph1 and Sph2) demonstrates a mutual inclusion relationship. The nature of this relationship from core to rim and their similar sulphur isotope values (5.5–8.3 ‰) indicates a single sulphur source, suggesting that the different mineralization types are the result of different stages of a continuous hydrothermal system. Sphalerite geothermometer study suggests that sphalerite in the Tianbaoshan deposit formed in a low-temperature (<200 °C) hydrothermal system. The low concentrations of Mn and In, low In/Ge ratios and high Fe/Cd ratios in the sphalerite are consistent with those of Mississippi Valley-type (MVT) deposits, but different from those of magmatism-related deposits (e.g. epithermal, skarn and VMS deposits). The positive  $\delta^{34}\text{S}$  values for Py1 (5.1–7.9 ‰), Cp1 (5.1–7.2 ‰), Sph1 (4.7–7.4 ‰), Sph2 (3.9–8.7 ‰), Py2 (4.4–9.3 ‰) and Cp2 (5.0–6.8 ‰) indicate a sulphur source from thermochemical reduction of coeval seawater sulphate. Widely developed dissolved textures (caverns and breccias) with massive sulphide infillings and deformed host rock remnants suggest that replacement of host dolostones by ore fluids was volumetrically significant and the ore formed nearly simultaneously with the cavities. The Tianbaoshan deposit is a typical MVT deposit, which resulted from mixing of a H<sub>2</sub>S-rich fluid and a metal-rich fluid, with thermochemical sulphate reduction occurring before ore precipitation rather than during ore precipitation.

**1. Introduction**

The Sichuan–Yunnan–Guizhou (SYG) triangle area belongs to the low-temperature metallogenic domain in South China (Tu, 2002; Hu & Zhou, 2012). This region, geologically located in the western Yangtze Block (Fig. 1a), is bounded by the NW–SE-trending Weining–Shuicheng fault to the northeast, the N–S-trending Anninghe fault to the west, and the NE–SW-trending Mile–Shizong fault to the southeast (Fig. 1b). It hosts more than 400 Pb–Zn deposits with >20 Mt Pb + Zn metal resources (e.g. the world-class Huize deposit, the large Tianbaoshan and Daliangzi deposits; Fig. 1b), and constitutes a world-class Pb–Zn metallogenic province (Hu & Zhou, 2012; Zhang *et al.*, 2015a). The ore-bearing strata of the Pb–Zn deposits in this region are located below the Permian Emeishan basalts and include Sinian to Permian carbonate strata, among which the Sinian–Cambrian stratum is the most important ore-bearing stratum in the area. Regional Pb–Zn deposits are characterized by epigenesis and are typical Mississippi Valley-type (MVT) in terms of mineral assemblage, mineralization type, lithology of ore-bearing strata and wall rock alteration (Han *et al.* 2007; Zhang, 2008; Wu, 2013; Zhang *et al.* 2015). However, most Pb–Zn deposits in this area are different from typical MVT deposits in terms of orebody

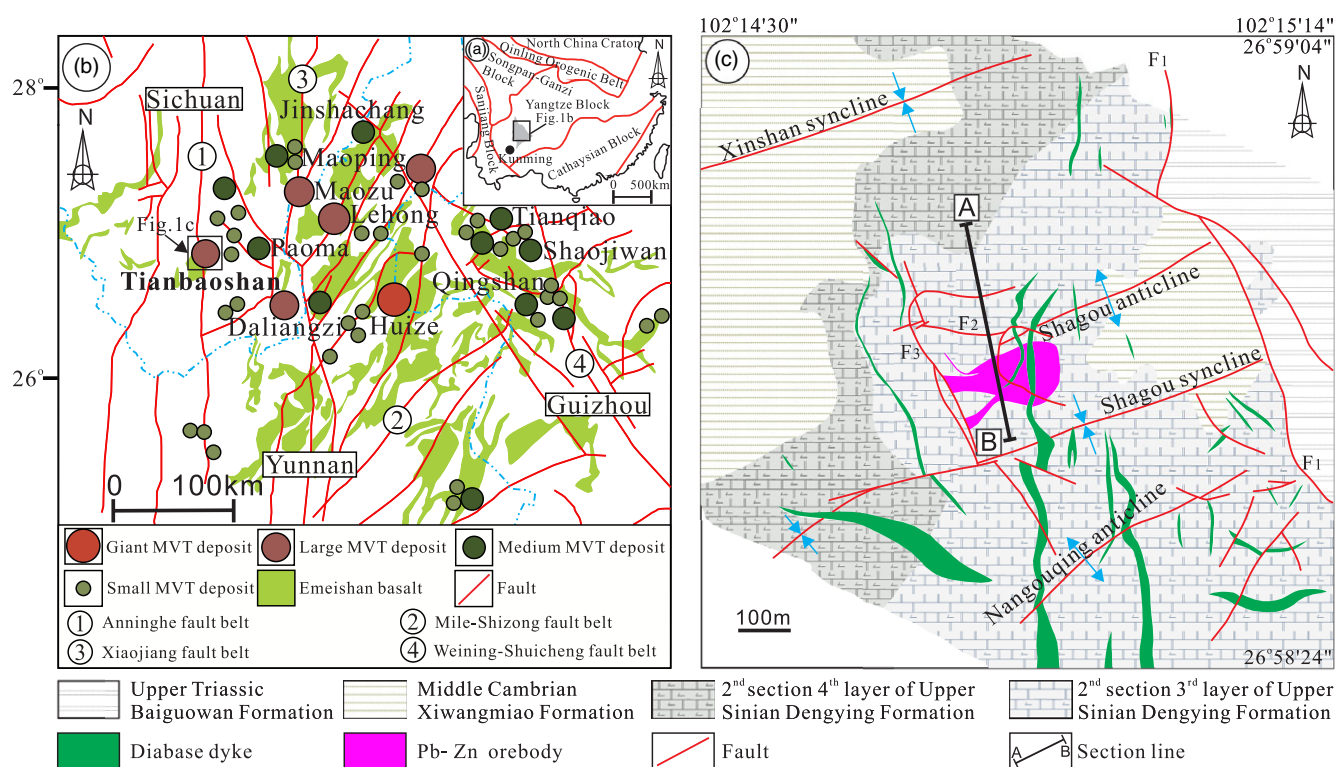


**Fig. 1.** (Colour online) (a) Tectonic sketch of South China. (b) Schematic regional geological map of the Sichuan–Yunnan–Guizhou MVT triangle region showing the distribution of principal deposits modified from Zhang *et al.* (2015); small box shows location of (c). (c) Geological sketch map of the Tianbao ore segment within the Tianbaoshan deposit; the studied cross-section (line 30) of the orebody is also shown.

shape, ore-controlling factors and ore grade. Their formation is controlled by faults. They are vein-like in morphology and have generally very high ore grades with more than 20 % Pb and Zn, such as the Huize (Han *et al.* 2007), Maoping (Wei *et al.* 2015) and Fule deposits (Zhu *et al.* 2017; Li *et al.* 2018). Additionally, copper-bearing minerals are not generally common in MVT deposits (Symons *et al.* 2009; Abidi *et al.* 2010), and copper sulphides have only been discovered in a few MVT deposits (Pfaff *et al.* 2009; Muhling *et al.* 2012). In contrast, such an association is common in many Pb–Zn deposits (e.g. Wushihe, Maozu and Chipu deposits) in the SYG area (Zhang *et al.* 2005) and many copper ore occurrences have been discovered in the Permian basalt (Wang & Wang, 2003; Li *et al.* 2004; Wang *et al.* 2010; Zhang *et al.* 2015). However, an understanding of the relationship between lead–zinc and copper mineralization still lacks geological and geochemical evidence (Tan *et al.* 2019). Although the classification of these deposits has been changed from sedimentary type (Tu, 1984; Chen, 1986; Liu & Lin, 1999) to MVT type (Zhou *et al.* 2001; Han *et al.* 2007; Hu & Zhou, 2012), their unique geological characteristics suggest that the lead–zinc mineralization has a complex origin (Zhou *et al.* 2013, 2014, 2018; Li *et al.* 2015; Wang *et al.* 2018; Tan *et al.* 2019) and needs to be further studied.

Here we present an example of the association of Cu and Pb–Zn in the Tianbaoshan ore deposit. This deposit comprises three separated vein orebodies, Tianbao I, Tianbao II and Xianshan, of which Tianbao II is the largest. Ore reserves total ~26 Mt Zn and Pb (grading 7.76–10.09 % and 1.28–1.50 %, respectively; Ye *et al.* 2016). Recently, a Cu orebody was discovered below the Pb–Zn orebody, which has >0.1 Mt Cu ore reserves and a mean grade of 2.55 wt % Cu (Tan *et al.* 2019). Previous studies have been carried out on the ore deposit's geological features (Feng *et al.* 2009;

Cheng, 2013), fluid inclusions and C–H–O–He–Ar isotopes (Wang, 1992; XC Wang *et al.* 2000; Yu *et al.* 2015; J Wang *et al.* 2018; Yang *et al.* 2018), trace elements in sulphides (Wang, 1992; Wang *et al.* 2000; Ye *et al.* 2016; Hu *et al.* 2018), and S–Pb–Cd isotopes of sulphides (Sun *et al.* 2016; Zhu *et al.*, 2016; Tan *et al.* 2019). These workers suggested that the ore-forming process of the Tianbaoshan deposit is either non-magmatic mineralization (e.g. MVT type; Wang, 1992; Wang *et al.* 2000; Yu *et al.* 2015; Ye *et al.* 2016; Hu *et al.* 2018; Wang *et al.* 2018; Yang *et al.* 2018) or mineralization related to magmatism (SYG type; Zhu *et al.* 2016; Tan *et al.* 2019). The precipitation mechanism of metals is still controversial and the relationship between Pb–Zn and Cu mineralization in the deposit remains unclear.

Geochemical signatures of sulphide minerals (e.g. pyrite, sphalerite and chalcopyrite) can reveal metallogenic information. For example, they allow us to distinguish between a single-stage event and multiple overprints (Yuan *et al.* 2018; Cave *et al.* 2020), differentiating metallogenic types (e.g. VHMS-type, skarn-type, MVT-type; Ye *et al.* 2011; Leng *et al.* 2018; Yuan *et al.* 2018; Niroomand *et al.* 2019; Xiao & Li, 2019; Zhuang *et al.* 2019; Oyebamiji *et al.* 2020), and constraining physicochemical conditions (e.g. T, pH,  $fO_2$ ) of the hydrothermal fluid (Hu *et al.* 2018; Leng *et al.* 2018; Horn *et al.* 2019; Maurer *et al.* 2019; Zhuang *et al.* 2019; Cave *et al.* 2020; Knorsch *et al.* 2020).

The sulphur isotopic signatures of the sulphide minerals (e.g. pyrite, sphalerite and chalcopyrite) can constrain the mechanisms of metal precipitation, particularly regarding Pb–Zn mineralization hosted by carbonate rocks. It has been suggested that the main sulphur sources for carbonate-hosted Pb–Zn deposits generally include evaporite-derived sulphur (heavy  $\delta^{34}S$  values), previously deposited bacteriogenic sulphur (light  $\delta^{34}S$  values) and

magma-derived sulphur (intermediate  $\delta^{34}\text{S}$  values) (Perona *et al.*, 2018; Elliott *et al.* 2019). Although a change in physicochemical conditions (e.g. T, pH and  $f\text{O}_2$ ) of a single hydrothermal fluid could cause sulphide precipitation, mostly sulphide mineralization is related to mixing of at least two fluids with contrasting components (e.g. sulphur-rich, metal-depleted brine and metal-rich, sulphur-poor hydrothermal fluid) (Ashton *et al.*, 1998; Blakeman *et al.* 2002; Wilkinson *et al.* 2005; Bouabdellah *et al.* 2008, 2012; Barrie *et al.* 2009; Gagnevin *et al.* 2014; Saintilan *et al.* 2015; Elliott *et al.* 2019). Compared to conventional bulk sulphur isotopic analysis, microscale variations in sulphur isotopes obtained by *in situ* analysis of sulphide minerals reveal more details of mineralizing processes (Deloule *et al.* 1986; Layne *et al.* 1991; McKibben & Eldridge, 1995; Peevler *et al.* 2003; Ferrini *et al.* 2010).

In this contribution, we present a detailed study of ore and mineral textures, coupled with *in situ* trace-element and sulphur isotopic analyses for sulphides from different-stage ores, to better address the mineralization mechanism of the sulphides and the link between Pb–Zn and Cu mineralization.

## 2. Geological setting

### 2.1. Regional geology

The SYG region is mainly composed of a pre-Sinian basement, Sinian to Palaeozoic marine sedimentary sequences and Mesozoic to Cenozoic terrestrial sedimentary sequences (Zhang *et al.*, 2019a). The basement in this region includes the Kangding, Dahongshan and Kunyang groups that mainly consist of gneiss, migmatite, meta-clastics, clastic rocks and minor carbonates (Zhou *et al.* 2001; Wu *et al.*, 2013). Sinian to Palaeozoic marine sedimentary sequences that cover the basement rocks consist of the lower Sinian acidic, intermediate-acidic igneous rock suite, the upper Sinian Dengying Formation dolostone and the Palaeozoic carbonates and clastic sediments, which are overlain by the voluminous Permian Emeishan flood basalts (Zhang *et al.* 2015). The Mesozoic to Cenozoic terrestrial sedimentary sequences are mainly sandstones and conglomerates, which are characterized by an entirely continental origin (Zhou *et al.* 2014; Zhang *et al.* 2015). The upper Sinian Dengying Formation is the most important ore-hosting stratum in the SYG, accounting for over 75 % of the Zn + Pb reserves (Zhang *et al.*, 2019b). Carbonate-hosted Zn–Pb deposits, such as the Chipu, Maozu, Daliangzi, Tianbaoshan, Tianqiao Shaojiwan and Qingshan deposits, are distributed along the Anninghe, Weining–Shuicheng and Mile–Shizong regional faults and their secondary faults (Fig. 1b; Zhang *et al.* 2015; Zhang *et al.*, 2019a, 2019b). These regional faults commonly control the migration of regional ore-forming fluids, and a series of thrust–fold systems are the primary ore-hosting structures in the SYG, where sulphide orebodies are generally present as strata-bound lenses in bedding-parallel fractures or as pipe-like orebodies (Zhang *et al.* 2015; Xiong *et al.*, 2018; Zhang *et al.*, 2019a, 2019b). These Zn–Pb deposits were formed at 245–225 Ma, co-temporally with the collision between the Indochina and South China cratons, and the Zn–Pb mineralization is genetically related to the regional-scale migration of basin-related fluids triggered by the late Indosinian orogeny (Hu & Zhou, 2012; Zhang *et al.* 2015).

### 2.2. Local geology

The Tianbaoshan Pb–Zn deposit is hosted by dolostone of the upper Sinian Dengying Formation, which consists of the

Tianbao and Xinshan ore segments (Wang *et al.* 2000; Hu *et al.* 2018; Tan *et al.*, 2019). This study focuses on the Tianbao ore segment. The major strata exposed in the Tianbao ore segment include the upper Sinian Dengying Formation, the Middle Cambrian Xiwangmiao Formation and the upper Triassic Baiguowan Formation (Fig. 1c; Zhou *et al.* 2013; Hu *et al.* 2018). The Dengying Formation consists of four layers (Tan *et al.* 2019): the first layer, up to 320 m thick, consists of dolostone; the second layer is composed of a 32–112 m thick dolomitic sandstone; the third layer comprises 240–470 m of siliceous dolostone, which is the host rock for Pb–Zn mineralization; and the fourth layer consists of siliceous dolostone with chert strips or nodules (30–110 m thick). The first and second layers are absent in the Tianbao ore segment, while the third and fourth layers are widely developed in this area (Fig. 1c). The overlying Xiwangmiao Formation consists of clastic rocks, dominated by black shale of <210 m thickness, while the Baiguowan Formation is composed of sandy shale (40–200 m thick) (Zhou *et al.* 2013; Tan *et al.* 2019). Faults in this region mainly consist of N–S-, E–W- and NW-trending faults (Tan *et al.* 2019). The N–S-trending fault (F1 in Fig. 1c) in the eastern part of the ore district is the main ore-controlling structure that acted as conduits for ore-forming fluids. The E–W-trending fault (F2 in Fig. 1c) is the main ore-bearing structure which controls the occurrence of the Tianbaoshan deposit. The NW-trending fault (F3 in Fig. 1c) cross-cuts the orebodies. The Tianbaoshan syncline is a wide, asymmetrical composite syncline with a steep north limb (Fig. 1c; Tan *et al.* 2019). A series of secondary folds occurs in the two wings of the Tianbaoshan syncline, including the Xinshan syncline, the Shagou anticline and syncline and the Nangouqing anticline in the Tianbao ore section (Fig. 1c). Previous studies suggested that the Tianbaoshan area has undergone two episodes of regional compression in nearly NWW–SEE and SSW–NNE directions, which occurred in the late Indosinian and early Yanshanian, respectively (Zhang *et al.*, 2006; Tan *et al.* 2019). The Pb–Zn mineralization in Tianbaoshan is considered to be linked to the late Indosinian regional compression (Zhang *et al.*, 2006). There is a lack of magmatic activity in the Tianbaoshan area, with only several diabase dykes occurring along N–S-trending and NW-trending faults (Fig. 1c). These mafic dykes with a thickness of 20–30 m usually cross-cut the orebodies (Fig. 1c) and were dated by Zhang (2017) at 156–166 Ma. In the contact zone between diabase dyke and orebody, the Zn + Pb grade of the orebody increases and the dyke itself is a high-grade Zn–Pb orebody (Cai, 2012; Zhang, 2017).

### 2.3. Ore deposit geology

The Tianbaoshan deposit contains three orebodies including two Tianbao orebodies (Nos. I and II) and one Xinshan orebody (No. III) (Wang *et al.* 2000; Feng *et al.* 2009; Tan *et al.* 2019). The No. II orebody is the largest within the Tianbaoshan ore district, with average grades of 1.09 wt % Pb and 8.74 wt % Zn. This Pb–Zn orebody is more than 300 m thick, ~285 m long and ~70 m wide, and is cross-cut by the NW-trending fault which forms two ore segments (Yang *et al.* 2018). They are structurally controlled by the E–W-striking faults and hosted in siliceous dolostone of the third layer of the Dengying Formation, which commonly occurs as steeply dipping, lens-shaped and in sharp contact with the siliceous dolostone host rock (Figs 2, 3a; Hu *et al.* 2018; Tan *et al.* 2019). Recently, Cu-dominant mineralization was discovered in the deep part of the Tianbaoshan deposit and forms a Cu orebody (Fig. 2). The Cu orebody has a lenticular form in the Tianbao orebodies, is

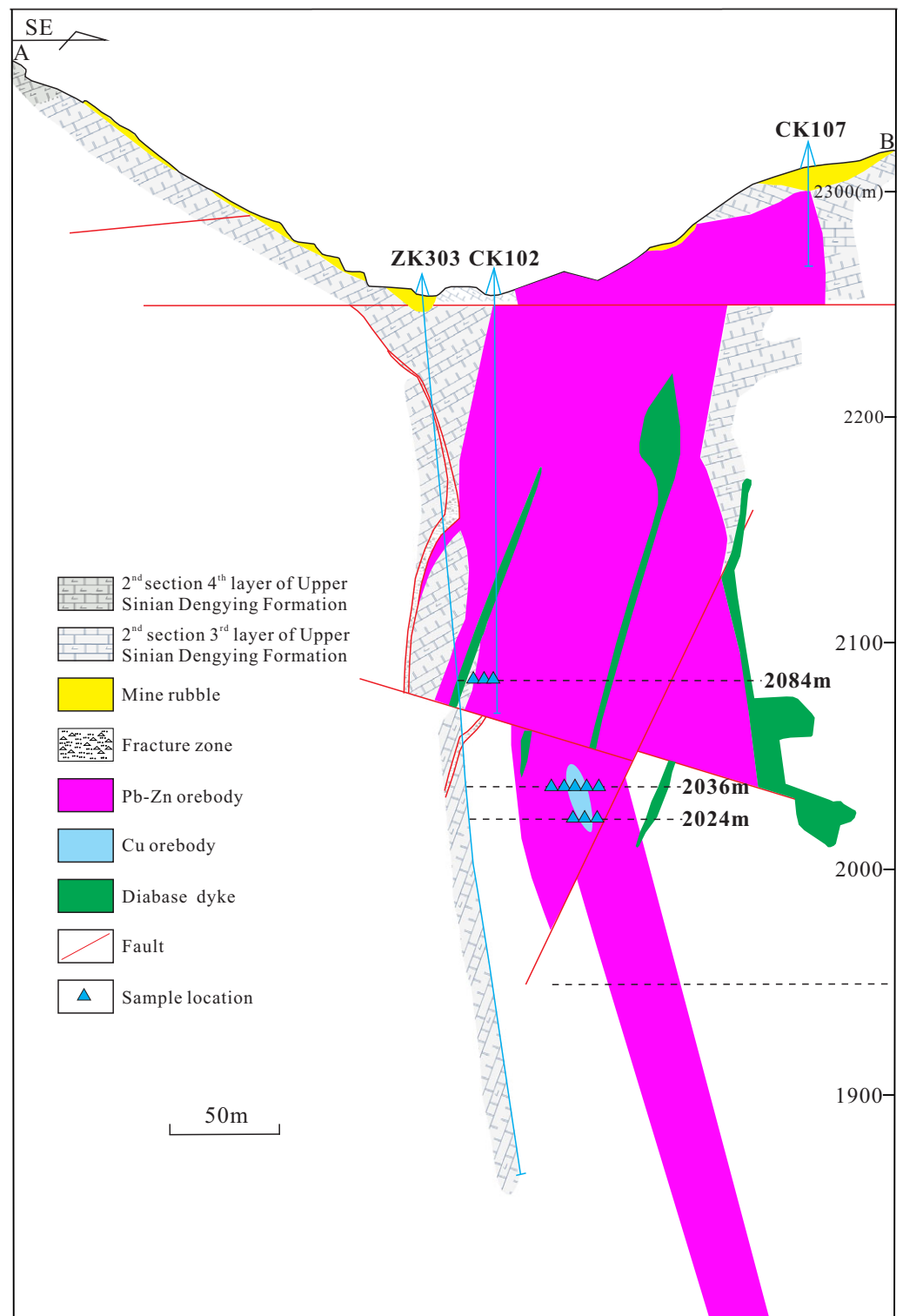


**Fig. 2.** (Colour online) Geological cross-section along the No. 30 exploration line.

found at an elevation of 2036 m (Fig. 3b–c) and thins out at 2024 m (Fig. 3d). It dips south, has a length of up to 50 m and is ~10 m thick (Hu *et al.* 2018; Tan *et al.* 2019). This orebody contains over 100 000 tons of Cu ores at an average grade of 2.55 % Cu (Tan *et al.* 2019). The sulphide ores are relatively simple and predominantly consist of sphalerite with minor galena, pyrite and chalcopyrite. The gangue minerals are dominated by dolomite, calcite and

quartz (Wang *et al.* 2000; Feng *et al.* 2009; Sun *et al.* 2016; Ye *et al.* 2016).

### 3. Sulphide minerals petrography

Detailed mineralogical and textural investigations of samples from the Tianbaoshan orebody allow the splitting of the processes that

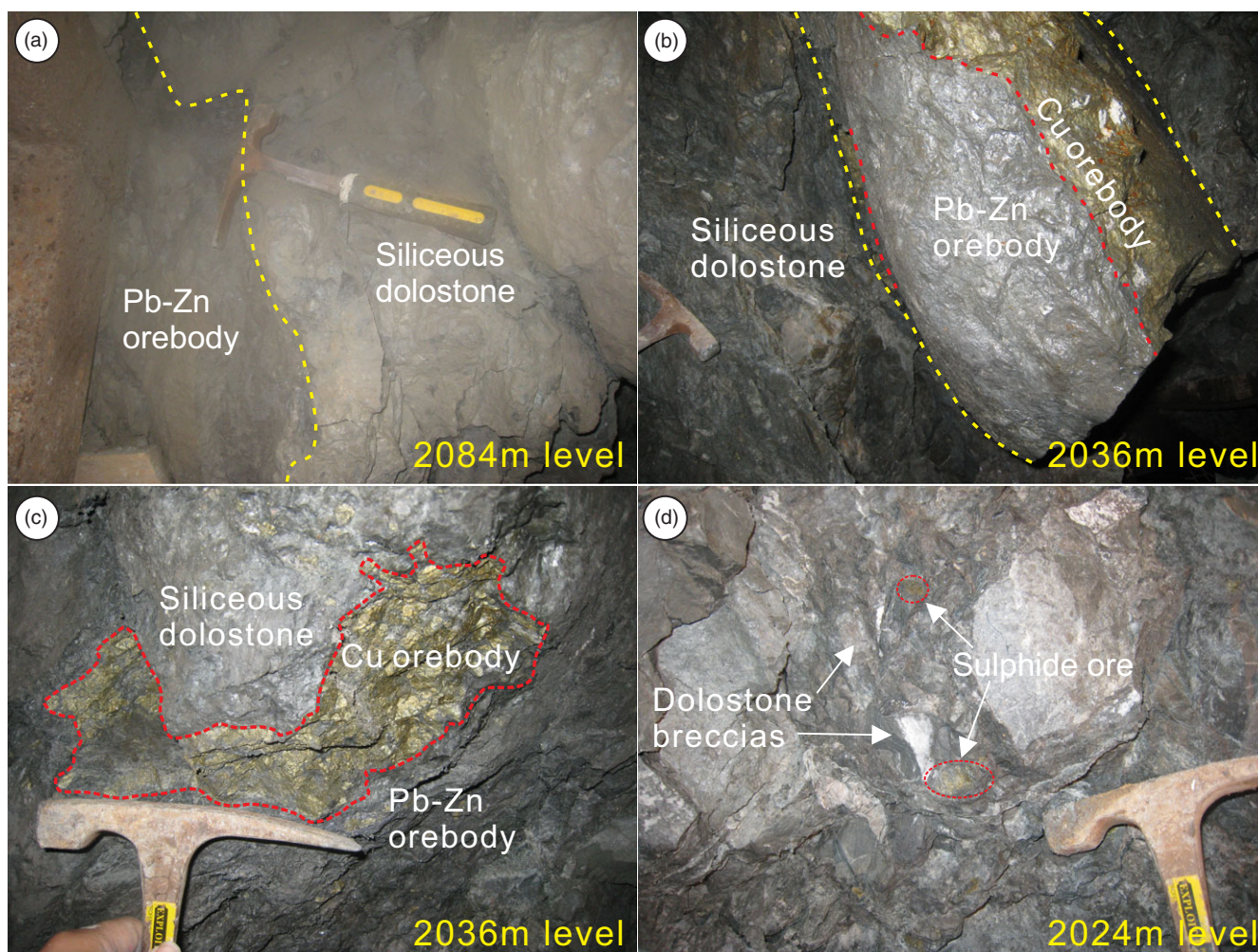


**Fig. 3.** (Colour online) Photographs of Pb–Zn and Cu mineralization occurrences from 2084 m, 2036 m and 2024 m a.s.l. in the Tianbao No. II orebody. (a) The 2084 m level shows sharp contact between Pb–Zn orebody and siliceous dolostone host rocks. (b–c) The 2036 m level shows a minor Cu orebody occurring as lenticular form in the massive Pb–Zn orebody. (d) The 2024 m level shows brecciation of dolostone host rock with minor sulphide infillings, and that the Cu orebody tends to thin out at this level.

formed the deposit into early pyrite, early chalcopyrite, the main sphalerite, and carbonate stages (Fig. 4).

### 3.1. Early pyrite stage (Stage 1)

In this stage, pyrite patches were developed in the brecciated ore (Fig. 5c) or massive sulphide ore (Fig. 5d). These pyrite patches (Py1) occur in small quantities relative to other sulphides during whole stage, and are only observed in rare ore specimens. In thin-sections, the crystals of Py1 are highly fractured and appear as anhedral to subhedral 80–800  $\mu\text{m}$  relic crystals (Figs 6b, d, 7a). They have a porous or cracked surface with infillings of carbonate or sulphide minerals (Figs 6b, d, 7a). This type of pyrite was intensively replaced by chalcopyrite (Fig. 6b, d) or sphalerite (Fig. 7a) along its rims or internal fractures. Therefore, pyrite in this stage is the earliest sulphide mineral, predating subsequent sulphides.

### 3.2. Early chalcopyrite stage (Stage 2)

The second stage of the mineral phase is dominated by chalcopyrite mineralization occurring as disseminated grains (Fig. 5c–d). It commonly replaced early Py1 patches or is surrounded by massive sphalerite grains (Fig. 5c–d). It also occurs as coarse-grained,

elliptical crystals (Cp1) (Fig. 6b, d) and encloses the early Py1. The Cp1 is surrounded by dark sphalerite (Sph1) that exhibits irregular boundaries, suggesting that Cp1 formed earlier than the Sph1 (Fig. 6b, d).

### 3.3. The main sphalerite stage (Stage 3)

Abundant sulphide mineralization took place in this stage and the sulphide mineralogy is simple sphalerite. It occurs as massive (Fig. 5a–b, d) and brecciated textures (Fig. 5c, e–f), which intensively replaced the dolomite host rock or filled between wall rock breccia. Two types of sphalerite are identified based on microscopic textural characteristics as follows: (a) early dark fine-grained sphalerite (Sph1) and (b) late light coarse-grained sphalerite (Sph2). The Sph1 around elliptical Cp1 is present as dark-coloured, anhedral fine-grained crystals (Figs 6, 7a), and is typified by a large quantity of dusty chalcopyrite disease condensing into larger particles (Fig. 6b, d, f, g). It is noted that these chalcopyrite blebs are only observed within Sph1. Sph1 is also widely distributed throughout the host rock, accompanied by significant silicification (Fig. 6e–h). In contrast, the Sph2 around Sph1 appears as light-coloured, coarse-grained crystals, and lacks chalcopyrite disease (Figs 6b, d, 7b–f). In some cases, the Sph2 cross-cuts the Sph1

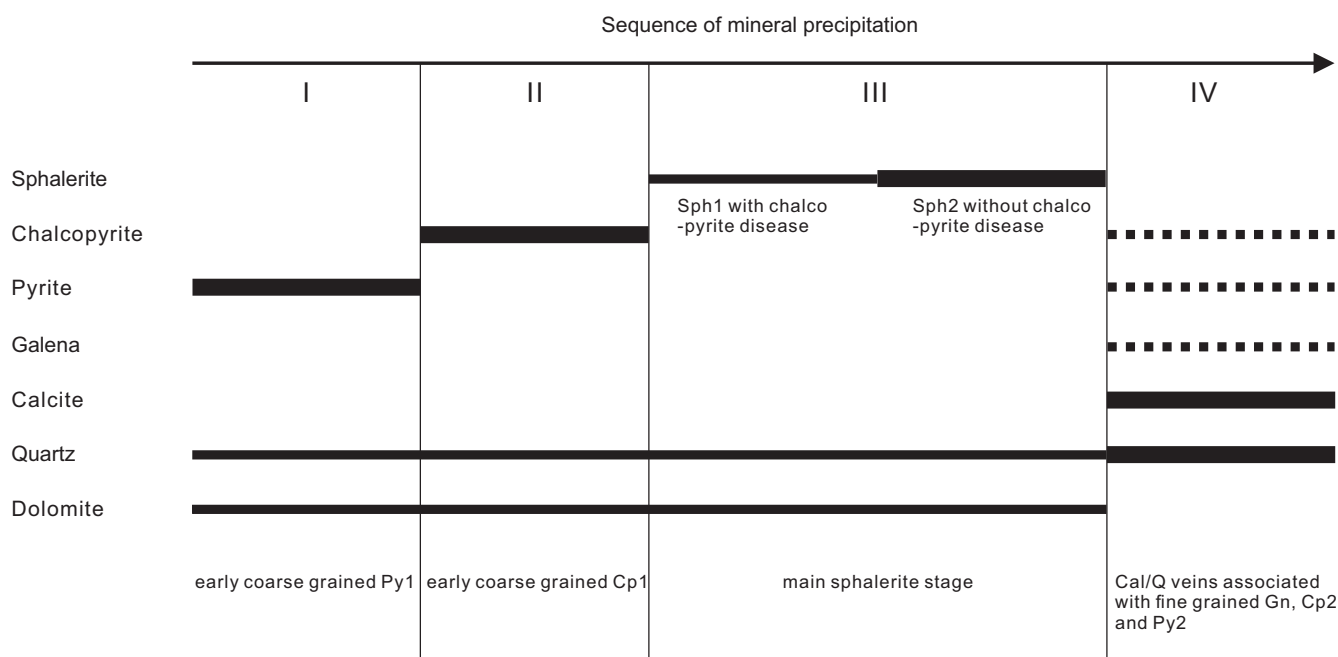


Fig. 4. Paragenetic sequence of sulphide and associated alteration mineral formation in the Tianbaoshan deposit.

as veinlets (Fig. 6e–g). Sph2 formation occurs in large quantities relative to Sph1 during the main mineralization stage.

### 3.4. Carbonate stage (Stage 4)

The late stage of the hydrothermal phase is characterized by calcite and quartz, with rare sulphide mineralization, including galena, pyrite and chalcopyrite as caverns and fracture-filling veins in massive ores (Fig. 5a–b, d, f). In thin-sections, the pyrite (Py2), chalcopyrite (Cp2) and galena of Stage 4 are closely associated with veins of calcite and quartz, and occur as veinlets or fine-grained crystals that cut or replaced previous sulphide phases. Chalcopyrite (Cp2) exhibits anhedral, fine-grained forms filling between Sph1 (Fig. 6f) or Py1 (Fig. 7a) grains. Py2 shows veinlets cross-cutting coarse-grained Sph2 (Fig. 7b–f). Noticeably, some veinlets of fahlore have intergrowth textures with Cp2, which cross-cut both Sph1 and Sph2 (Fig. 6f–g). The galena coexists with Py2, quartz and calcite, which cross-cuts Sph2 as veinlets (Figs 6d, 7f).

## 4. Sampling and methods

Sulphide ore samples were collected from three different levels (2024 m, 2036 m and 2084 m) in the Tianbao No. 2 orebody. Double-polished petrographic thin-sections were first studied using both transmitted and reflected light to distinguish the four paragenetic stages (1–4) of sulphides. After a detailed preliminary petrographic study, locations suitable for laser ablation – inductively coupled plasma – mass spectrometry (LA-ICP-MS) analysis were selected with surfaces free from scratches, no visible inclusions and no microfractures visible on the surface. Six polished thin-sections of representative sulphide minerals (pyrite, chalcopyrite and sphalerite) from each of the four paragenetic stages were then used to analyse major and trace elements and subsequent sulphur isotopes using LA-ICP-MS. The areas selected for sulphur

isotope analysis were approximated to the major and trace element analysis points.

### 4.1. LA-ICP-MS analysis for trace elements

*In situ* trace elements were analysed using a Photon Machines Excite Excimer laser ablation system coupled to an Agilent 7700x quadrupole ICP-MS at the Nanjing FocuMS Technology Co. Ltd. An energy density of  $6.06 \text{ J cm}^{-2}$  and a repetition rate of 6 Hz were used with laser spots 40  $\mu\text{m}$  in diameter for sample analysis. Helium carrier gas was used to transport the aerosol, and was mixed with argon via a T-connector before entering the ICP-MS. The total 55 s analysis time included a 15 s background measurement before ablation. The 8:3 standard sample bracketing approach (three standard samples analysed twice every eight unknowns) was used to correct for mass bias and instrument drift. An in-house standard pure pyrite was used for calibration of the concentrations of S and Fe. The integrated count data of concentrations for other elements were calibrated by US Geological Survey (USGS) synthetic basaltic glass GSE-1G. The USGS sulphide reference material MASS-1 was analysed as an unknown sample to check the analytical accuracy. The preferred values of element concentrations for the USGS reference glasses were from the GeoReM database (<http://georem.mpch-mainz.gwdg.de/>). Raw data reduction was performed offline by ICPMSDataCal software using 100 %-normalization strategy without applying an internal standard (Liu *et al.* 2008). The precision of each analysis is better than 15 % for most elements (>1 ppm).

### 4.2. LA-MC-ICP-MS analysis for sulphur isotopes

*In situ* sulphur isotope analyses of sulphides were carried out using a 193 nm ArF excimer laser-ablation system coupled to a Nu Plasma II multi-collector MC-ICP-MS in the Nanjing FocuMS Technology Co. Ltd. An energy density of  $2.5 \text{ J cm}^{-2}$  and a repetition rate of 5 Hz were used with spot diameters of 33  $\mu\text{m}$ , 40  $\mu\text{m}$

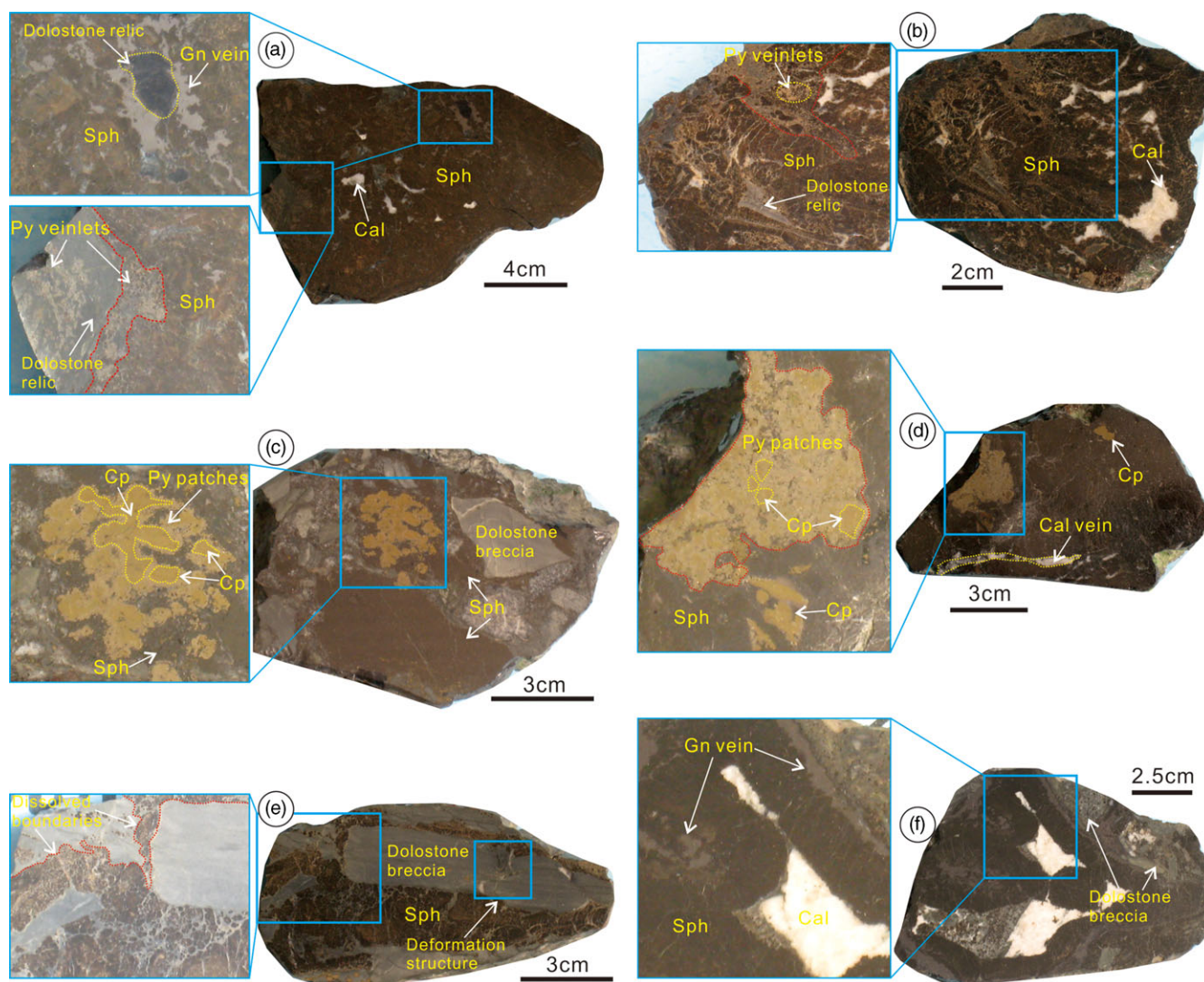


**Fig. 5.** (Colour online) Photographs of typical ore texture and mineral assemblage in the Tianbaoshan deposit. (a) Sphalerite–galena massive ore, which shows that galena and pyrite veinlets cross-cut massive ore, and rare dolostone relics are suspended in massive ore with some calcite infillings. (b) Dolostone relic-bearing massive sphalerite ore with pyrite and calcite veinlets filling along fractures. (c) Breccia-shaped sphalerite ore with sphalerite cementing dolostone breccias, which shows that pyrite patches overprint sphalerite and spot-like chalcopyrite replaces the pyrite patches. (d) Spot-like chalcopyrite either replaces pyrite patches or is enclosed by massive sphalerite with calcite vein filling along fracture. (e) Sphalerites cement the dolostone breccias with irregularly dissolved boundaries and deformation structure in the dolostone breccias. (f) Sphalerites occur as open space-filling texture among the dolostone breccias with calcite filling in the dissolution cavity of former sphalerite. Abbreviations: Py = pyrite; Sph = sphalerite; Cp = chalcopyrite; Gn = galena; Cal = calcite.

and 50  $\mu\text{m}$  for pyrite, sphalerite and chalcopyrite, respectively. Each analysis comprised 40 s of ablation for signal collection and 30 s for background measurement. Helium ( $800 \text{ mL min}^{-1}$ ) was applied as the carrier gas to efficiently transport the aerosol out of the ablation cell, and was mixed with argon ( $\sim 0.8 \text{ L min}^{-1}$ ) via T-connector before entering the ICP torch. Natural pyrite Wenshan ( $\delta^{34}\text{S} = +1.1 \text{ ‰ V-CDT}$ ) was used as an external bracketing standard every fourth analysis, which is used to correct for instrument drift and mass bias. Pressed powder pellets of pyrite GBW07267 and chalcopyrite GBW07268 ( $\delta^{34}\text{S} = +3.6 \text{ ‰}$  and  $-0.3 \text{ ‰}$ , respectively, from National Research Center for Geoanalysis, China) and fine-grained sphalerite SRM 123 ( $\delta^{34}\text{S} = +17.5 \text{ ‰}$ , from National Institute of Standards and Technology, USA) were treated as quality-control samples. The long-term reproducibility of  $\delta^{34}\text{S}$  is better than  $0.6 \text{ ‰}$  (1 standard deviation).

## 5. Results

### 5.1. Mineral chemistry

The chemical compositions of various generations of pyrite, chalcopyrite and sphalerite from the Tianbaoshan deposit are determined by LA-ICP-MS. The summaries of the results of the pyrite (Py1 and Py2), chalcopyrite (Cp1 and Cp2) and sphalerite (Sph1 and Sph2) analyses are presented in Tables 1–3 and Figures 8–10, while the complete data are shown in Appendix 1 (in the Supplementary Material available online at <https://doi.org/10.1017/S0016756822001054>).

#### 5.1.1. Trace element characteristics of pyrites

Among the analysed elements, both Py1 and Py2 possess moderate concentrations of V, Cr, Co, Ga, Ge, As, Se, Ag, In, Sb, Te, Tl and Bi, with concentrations in the same order of magnitude (Table 1).

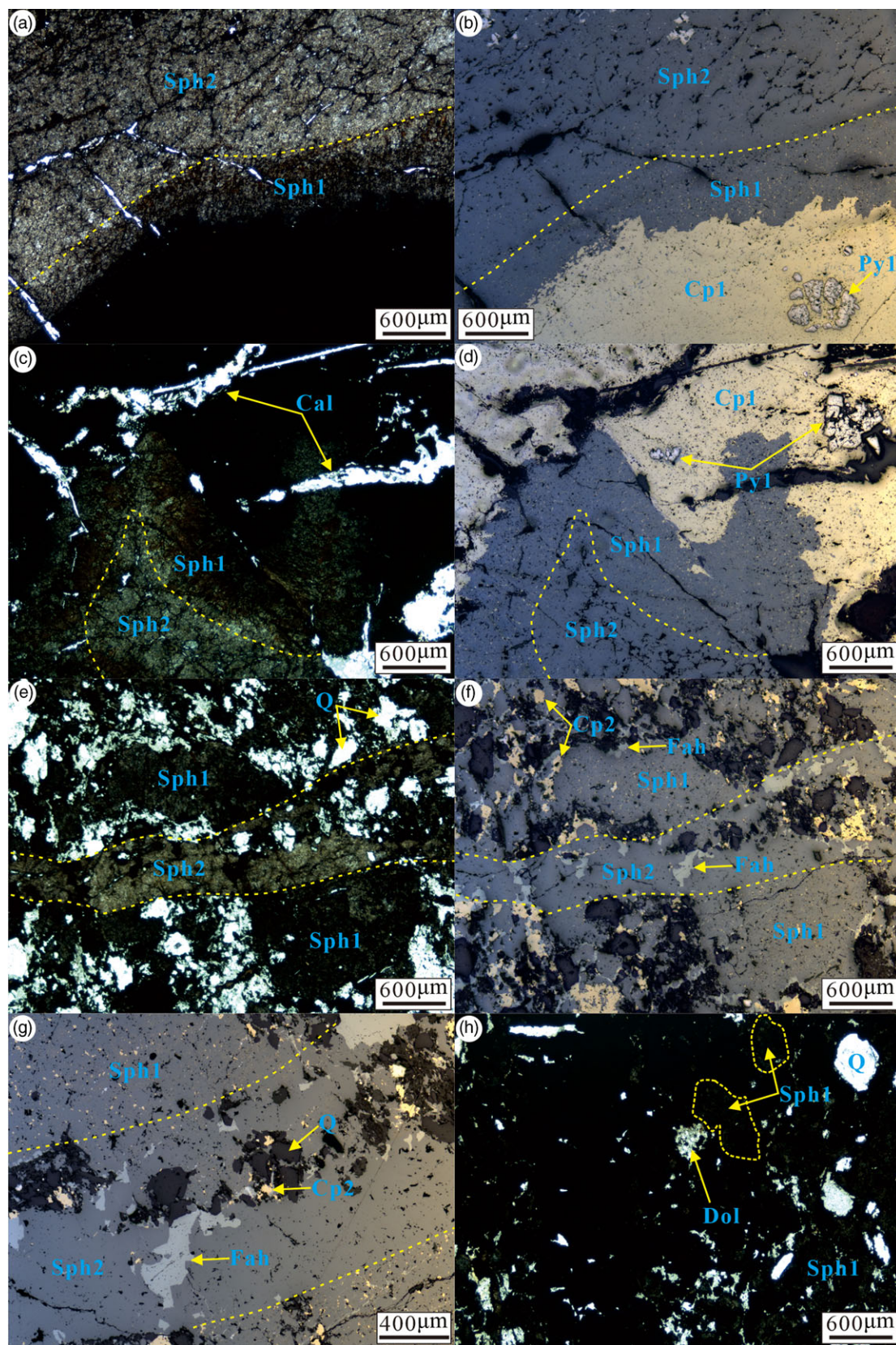


**Fig. 6.** (Colour online) Photomicrographs of sulphide mineral associations of early pyrite stage (Py1), early chalcopyrite stage (Cp1) and main sphalerite stage (Sph1 and Sph2) in the Tianbaoshan deposit. (a) Transmitted light microphoto shows that dark sphalerite (Sph1) is surrounded by light sphalerite (Sph2) with obvious boundary. (b) Reflected light microphoto from (a) shows Py1 relics occur in the chalcopyrite (Cp1) matrix, which was replaced by Sph1 with widespread chalcopyrite disease and Sph2 with rare chalcopyrite disease. (c–d) Both transmitted and reflected light microphotos show that two generation sphalerites (Sph1 and Sph2) replaced the early Cp1 grain enclosing relics of Py1 and formed a curved boundary between them. (e–f) The light Sph2 occurs as a veinlet cross-cutting composite aggregate of dark Sph1 with widespread chalcopyrite blebs, and anhedral fine-grained Cp2 and Fah crystals occur between massive Sph1 grains. (g) Details from (f), showing coexisting assemblage of fine-grained Q, Cp2 and Fah crystals, which replaced Sph2. (h) Transmitted light microphoto showing sulphide-bearing dolomite host rock has undergone silicification. Abbreviations: Py = pyrite; Cp = chalcopyrite; Sph = sphalerite; Fah = fahlore; Dol = dolomite; Q = quartz.



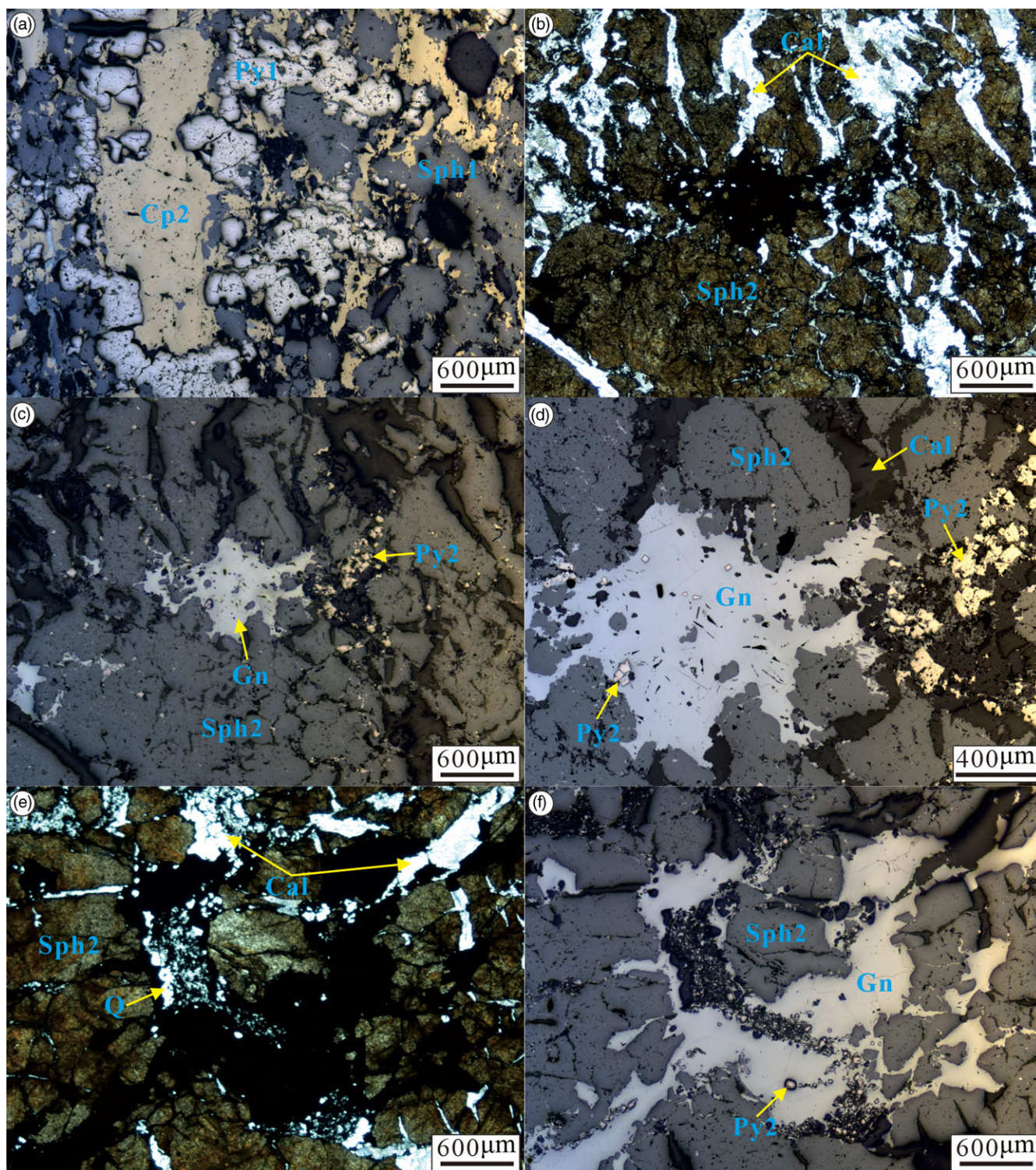


**Fig. 7.** (Colour online) Transmitted light photomicrographs and corresponding reflected light photomicrographs mainly showing sulphide mineral associations observed in the main sphalerite stage (Sph2) and carbonate stage from the Tianbaoshan deposit. (a) Reflected light microphoto from (h) in Figure 6 shows that the fractured Py1 grains are intensively replaced by massive Sph1 with siliceous dolostone relic, which is replaced by Cp2. (b–c) Coarse-grained sphalerite (Sph2) with no chalcopyrite disease is cut by pyrite (Py2) and calcite (Cal) veinlets. (d) Details from (c), anhedral fine-grained galena intergrown with pyrite and calcite, cross-cutting massive Sph2. (e–f) Fine-grained pyrites (Py2) disseminate in a galena (Gn) vein, together with calcite (Cal) and quartz (Q) veinlets, which cross-cut coarse-grained sphalerite (Sph2). Abbreviations: Py = pyrite; Sph = sphalerite; Gn = galena; Cal = calcite; Q = quartz.

The concentrations of Cu (mean = 1595 ppm), Zn (mean = 14 033 ppm) and Pb (mean = 19 302 ppm) are significantly higher in Py2 relative to Py1 (Table 1; Fig. 8).

#### 5.1.2. Trace element characteristics of chalcopyrites

Cp1 displays significantly high concentrations of Co (mean = 1199 ppm), Ni (mean = 577 ppm), As (mean = 4461 ppm), Mo

**Table 1.** Elemental compositions (in ppm) of different types of pyrites from the Tianbaoshan deposit

Element	Py1 ( <i>n</i> = 13)				Py2 ( <i>n</i> = 9)			
	Min	Max	Mean	SD	Min	Max	Mean	SD
V	0.13	2.39	0.71	0.67	0.11	2.16	0.88	0.75
Cr	8.05	76.3	34.3	19.3	1.74	102	34.3	32.0
Mn	0.58	38.2	5.02	10.3	0.55	164	20.1	54.1
Co	27.3	914	215	236	1.07	404	117	142
Ni	14.8	778	162	211	0.43	215	44.0	65.7
Cu	15.8	1199	635	349	32.5	4241	1595	1814
Zn	1.68	3165	549	872	1.25	50228	14033	16895
Ga	0.01	0.47	0.26	0.18	0.01	1.84	0.60	0.68
Ge	2.35	19.2	6.36	5.68	2.24	4.55	3.22	0.93
As	1264	8360	4812	2079	456	11429	5849	3907
Se	0.00	1.06	0.32	0.27	0.23	1.66	0.78	0.53
Mo	0.04	762	71.8	209	0.01	13.5	3.03	4.44
Ag	19.8	533	169	156	40.1	2914	466	951
Cd	0.57	32.0	8.17	8.99	1.20	126	50.9	48.2
In	0.00	0.13	0.03	0.05	0.00	0.51	0.07	0.16
Sb	7.71	834	208	223	63.1	1257	409	424
Te	0.00	0.07	0.01	0.02	0.00	0.039	0.01	0.01
Tl	0.02	0.44	0.12	0.12	0.00	0.156	0.07	0.05
Bi	0.04	1.12	0.28	0.37	0.01	0.954	0.23	0.31
Pb	1430	16 979	6686	5122	261	76 607	19302	29 237

(mean = 2734 ppm), Ag (mean = 1035 ppm) and Sb (mean = 1318 ppm) relative to Cp2 (Table 2). On the other hand, V, Mn, Ga, Ge, Se, Cd, In, Sn, Tl and Bi have low concentrations in both Cp1 and Cp2 (Table 2; Fig. 9). The contents of Cr (mean = 196 ppm) and Zn (mean = 8420 ppm) are significantly higher in Cp2 relative to Cp1 (Table 2).

### 5.1.3. Trace element characteristics of sphalerites

Almost all elements show a similar range of concentrations in the two sphalerite types (Table 3). V, Co, Ni, Mn, Se, Sb and Tl show a similar order of magnitude in the two sphalerite types (Table 3; Fig. 10). Notably, the contents of Cu (mean = 1852 ppm), As (mean = 101 ppm), Ag (mean = 212 ppm) and Pb (mean = 2185 ppm) in Sph1 are much higher than those of Sph2 (Table 3).

### 5.2. Sulphur isotope systematics

Sulphur isotope compositions of different types of pyrite, chalcopyrite and sphalerite are presented in Appendix 2 (in the Supplementary Material available online at <https://doi.org/10.1017/S0016756822001054>) and Figure 11. All sulphide minerals from the various mineralization stages define similar and positive isotopic signatures with  $\delta^{34}\text{S}$  values of *c.* 6.0 ‰, with a narrow range of 5.1 to 7.9 ‰ (average 6.2 ‰) for Py1, 4.4 to 9.3 ‰ (average 6.5 ‰) for Py2, 5.1 to 7.2 ‰ (average 6.0 ‰) for Cp1, 5.0 to 6.8 ‰ (average 5.8 ‰) for Cp2, 4.7 to 7.4 ‰ (average 5.8 ‰) for Sph1 and 3.9 to 8.7 ‰ (average 6.0 ‰) for Sph2 (Fig. 11).

## 6. Discussion

### 6.1. Link between Pb–Zn and Cu mineralization

The relationship between Pb–Zn and Cu mineralization has not been well constrained by previous studies.

The Py1 of Tianbaoshan is relatively rare compared with the other sulphide minerals and has been intensively overprinted by continuous hydrothermal sulphide deposition. It is only found as scarce relicts overprinted by Sph1 (Fig. 6b) or Cp1 (Fig. 6e). The Py1 grains occur between detrital grains (e.g. quartz) in the sandstone (Fig. 6b), and the rims of these grains including Py1 and quartz exhibit overgrowth of Sph1 (Fig. 6b), suggesting that the Py1 might represent the earliest expression of a hydrothermal ore fluid and offer nucleation sites for subsequent Cp1 and Sph1 growth. The relationship between Cp1 and Sph1 also exhibits similar characteristics. The minor Cu orebody is enclosed in the abundant Pb–Zn orebody without any cross-cutting relationship (Fig. 3b–c). Spot-like Cp1 grains surrounded by later dense sphalerite are observed in the massive sulphide ores (Fig. 5d) and they make up typical core–rim texture, with the core of elliptical chalcopyrite and the dark rim comprising fine-grained Sph1 (Fig. 6f–g), as previously reported by Hu *et al.* (2018) and Tan *et al.* (2019). Similarly, the light-coloured, coarse-grained Sph2 type overgrows surrounding Sph1 (Fig. 6f–g). The main sulphide minerals including Py1, Cp1, Sph1 and Sph2 demonstrate the sign of growth relationship from core to rim, suggesting that they were generated within a continuous hydrothermal system. This is confirmed by the homogeneous sulphur isotope signatures (5.5–8.3 ‰; Fig. 11) in ore minerals (pyrite, chalcopyrite and sphalerite).

**Table 2.** Elemental compositions (in ppm) of different types of chalcopyrites from the Tianbaoshan deposit

Element	Cp1 (n = 7)				Cp2 (n = 6)			
	Min	Max	Mean	SD	Min	Max	Mean	SD
V	0.13	1.58	0.46	0.54	0.21	9.23	4.56	4.28
Cr	0.00	16.90	3.63	6.00	3.91	967	196	381
Mn	0.47	32.9	8.35	11.9	0.16	18.8	6.85	7.17
Co	50.6	5564	1199	2070	3.32	219	103	93.4
Ni	3.52	2909	577	1104	0.56	42.4	10.7	16.1
Zn	159	23 080	4981	8343	127	27293	8420	10 607
Ga	0.15	0.35	0.24	0.08	0.31	6.68	4.22	2.19
Ge	1.65	17.0	10.0	7.51	5.26	14.3	8.21	3.27
As	440	12 990	4461	4485	289	1605	759	518
Se	0.45	2.43	1.48	0.69	0.81	2.17	1.50	0.53
Mo	8.78	7528	2734	3262	0.47	131	60.4	49.5
Ag	66.3	2527	1035	739	164	561	305	158
Cd	15.7	110	47.1	40.6	1.88	166	52.4	63.0
In	0.72	1.13	0.88	0.17	0.05	0.14	0.09	0.03
Sn	0.44	14.8	6.36	7.09	0.53	4.09	1.89	1.68
Sb	15.1	3222	1318	956	42.6	785	273	282
Tl	0.01	6.13	2.31	2.86	0.05	0.25	0.11	0.07
Bi	0.04	0.10	0.06	0.02	0.08	0.21	0.13	0.05
Pb	440	8162	3388	3395	101	17 287	7311	7407

with similar sulphur source affinity. Therefore, we suggest that the Cu and Pb–Zn ores should have formed in order from the same hydrothermal system.

### 6.2. Implications for genetic type of ore deposit

The genesis of the Tianbaoshan deposit has been equivocal and debated. It has been described as a magmatic hydrothermal deposit (e.g. a unique SYG-type: Zhou *et al.* 2013, 2018; Tan *et al.* 2019; a distal magmatic hydrothermal type: Xu *et al.* 2014) or as non-magmatic hydrothermal type (e.g. MVT: Wang 1992; Wang *et al.* 2000; Feng *et al.* 2009; Yu *et al.* 2015; Ye *et al.* 2016; Hu *et al.* 2018; Wang *et al.* 2018; Yang *et al.* 2018). However, the geological and mineralogical evidences of this study show that the carbonate-hosted Tianbaoshan Zn–Pb–Cu mineralization has many characteristics that are typical of MVT deposits (Sverjensky, 1986; Sangster, 1990; Leach *et al.* 2005, 2010).

The GGIMFis geothermometer of sphalerite (78–198 °C; Table 3) indicates that the ore-forming fluids responsible for Pb–Zn–Cu mineralization have an intermediate to low temperature. This signature is consistent with the temperature range of 75 to 200 °C typical of MVT deposits (Kesler *et al.* 1995; Leach *et al.* 2005, 2010; Fazli *et al.* 2019). Additionally, the trace element signature of sphalerite and pyrite in sediment-hosted Pb–Zn deposits can be used to effectively distinguish whether magmatic fluid has been added to a hydrothermal system. Previous studies (Cook *et al.* 2009; Ye *et al.* 2011) show that sphalerite from magmatic hydrothermal deposits (e.g. epithermal, skarn and VMS deposits) is typically characterized by elevated In, Sn, Mn, Co and Ga and low Ge and Cd contents, whereas that from non-magmatic or sedimentary deposits (e.g. MVT deposits) is typically

enriched in Ge and Cd, with low Mn, In, Co and Sn contents. In the discrimination diagrams of Fe–In/Ge, Fe/Cd–Mn, Co–Mn and In/Ge–Fe/Cd (Fig. 12), both stages of sphalerite from the Tianbaoshan deposit display similar elemental compositions to MVT-related sphalerite, but are distinct from sphalerite from high-temperature deposits (e.g. epithermal, skarn and VMS deposits) directly associated with magmatism and/or volcanism (Fig. 12). This suggests that the Tianbaoshan deposit is likely a MVT deposit which is not directly associated with magmatism and/or volcanism. Notably, the low-temperature hydrothermal fluid resembles basinal brines responsible for MVT deposits, as shown in the As–Co–Ni ternary diagram (Fig. 13).

Throughout the main Tianbaoshan orebodies, the predominant ore-controlling factors are the dolostone host rocks and the NNW-trending faults, which yield in wedge-shaped bodies with sharp boundaries with the host rocks (Fig. 3a–b). Due to the ore-controlling factors, the ores have textures that reflect replacement of the carbonate host rock and open space filling (Fig. 5) with a simple alteration style (silicification and carbonation), and contain a simple mineral assemblage, comprising sphalerite and minor chalcopyrite, pyrite and galena (Fig. 5). Moreover, there is a lack of igneous rocks in the Tianbaoshan area, except for few diabase dykes cross-cutting the sulphide orebodies (Figs 1d, 2). These features are typical of those observed in MVT deposits (Leach *et al.* 2005). Therefore, we suggest that the Tianbaoshan deposit is an MVT deposit and has no genetic relationship with magmatism.

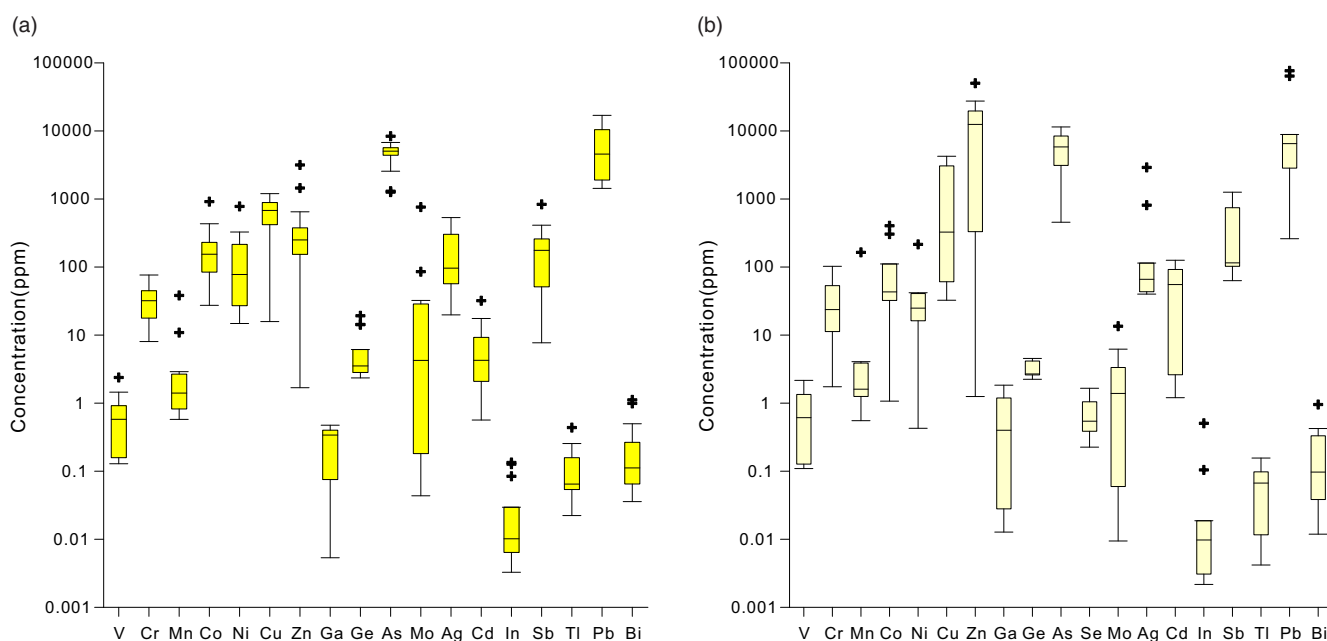
### 6.3. Fluid mixing as the main ore-forming process

A mixing model involving two different component fluids, a metal-rich solution and a H<sub>2</sub>S-rich solution, has frequently been

**Table 3.** Elemental compositions (in ppm) of different types of sphalerites from the Tianbaoshan deposit

Element	Sph1 (n = 9)				Sph2 (n = 12)			
	Min	Max	Mean	SD	Min	Max	Mean	SD
V	0.04	0.45	0.17	0.13	0.04	0.27	0.13	0.06
Cr	1.67	19.1	7.57	6.22	0.44	82.4	11.6	22.6
Fe	2057	4698	3408	917	1941	8994	5420	2423
Co	3.66	21.0	12.9	6.96	0.26	5.25	2.03	1.95
Ni	0.00	0.56	0.22	0.22	0.00	0.04	0.01	0.01
Cu	700	3637	1852	908	26	587	267	200
Ga	5.58	143	30.6	42.8	2.83	139	41.7	44.2
Ge	0.37	62.0	21.0	22.7	0.33	89.7	28.6	30.3
Mn	1.02	50.8	7.69	16.3	2.25	16.4	7.44	5.12
In	0.01	0.30	0.08	0.10	0.00	0.36	0.11	0.12
As	10.2	417	101	130	0.19	78.4	23.5	26.1
Se	0.52	0.81	0.66	0.13	0.41	1.08	0.60	0.18
Ag	126	560	212	135	30.3	259	98.1	74.5
Cd	2901	4957	3852	769	1236	3510	2129	888
Sn	0.45	12.8	2.25	4.02	0.14	25.7	4.06	7.38
Sb	41.1	386	147	110	4.01	299	84.3	96.7
Tl	0.00	0.21	0.04	0.07	0.00	0.04	0.01	0.01
Pb	176	8471	2185	3402	26.6	4006	649	1212
$T_{cal}$	78	167	120	34	92	198	130	36

Notes:  $T_{cal}$  means temperature was calculated using the formula suggested by Frenzel *et al.* (2016) (GGIMFis). LA-ICP-MS data of Ga, Ge, Mn, In and Fe were used during the calculation in this study.

**Fig. 8.** (Colour online) Boxplots of LA-ICP-MS results for trace element data of Py1 (a) and Py2 (b).

proposed to explain MVT ore deposition, which provides an important means of generating the large volumes of carbonate dissolution and sulphide precipitation in sedimentary carbonate rocks (Anderson & Garven, 1987; Ghazban *et al.* 1990; Mazzullo &

Harris, 1992; Qing & Mountjoy, 1994; Corbella *et al.* 2004). Previous studies (Samson & Russell, 1987; Maul, 1991; Banks & Russell, 1992; Eyre, 1998; Everett *et al.* 1999) suggest that the metal-rich fluid is characterized by low temperatures

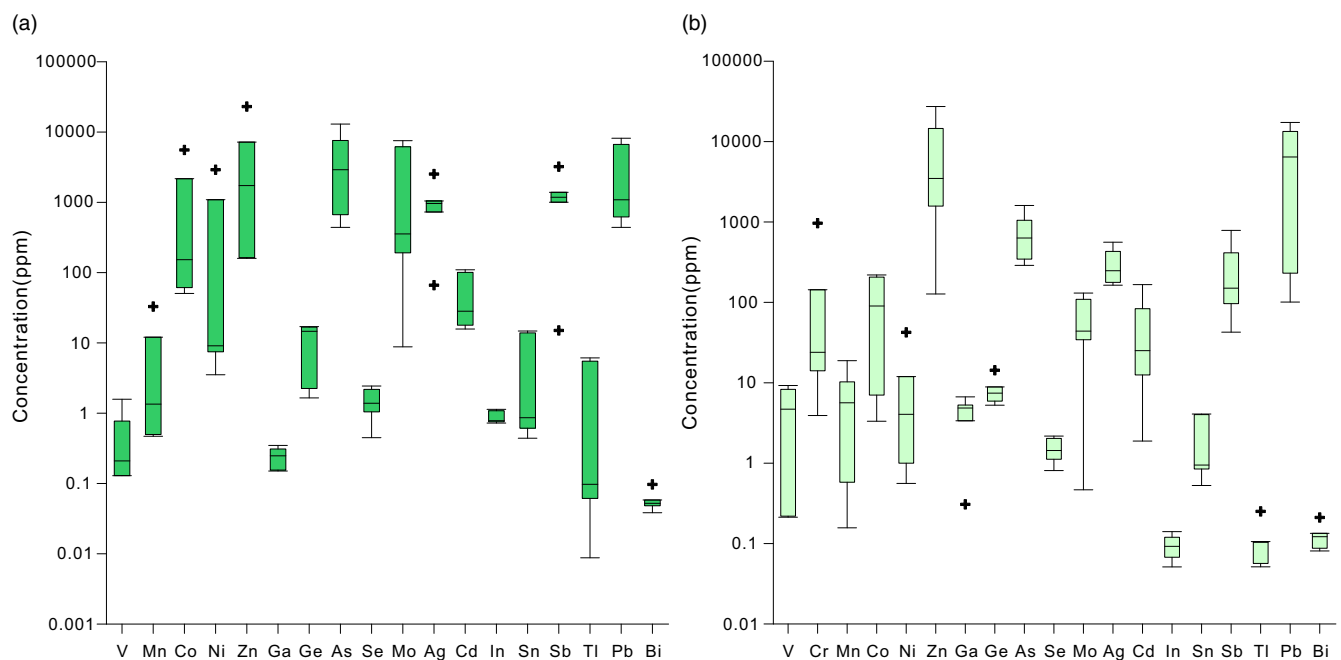


**Fig. 9.** (Colour online) Boxplots of LA-ICP-MS results for trace element data of Cp1 (a) and Cp2 (b).

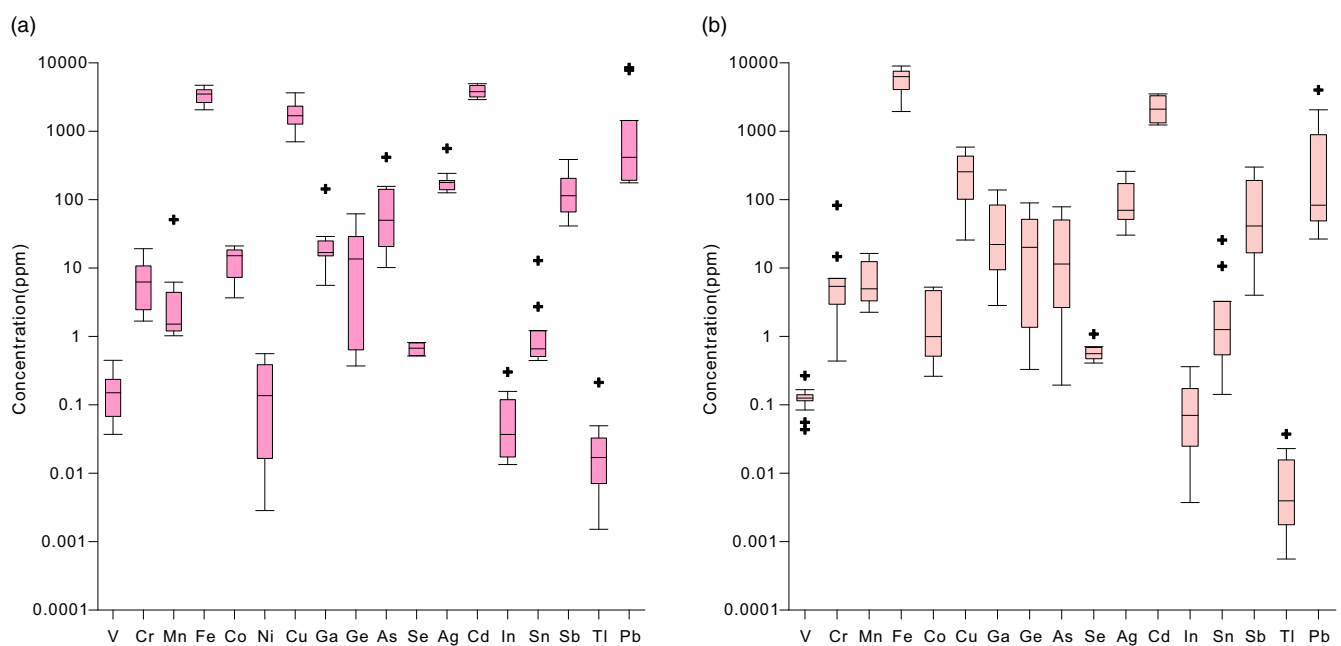


**Fig. 10.** (Colour online) Boxplots of LA-ICP-MS results for trace and minor element data of Sph1 (a) and Sph2 (b).

(70–120 °C) and high salinities (17–28 wt % NaCl equiv.) and that the H<sub>2</sub>S-rich fluid is characterized by middle-low temperatures (170–230 °C) and middle salinities (8–12 wt % NaCl equiv.). The former was considered to be a typical basinal brine (Leach, 1979; Coveney *et al.* 1987; Shelton *et al.*, 1992; Basuki & Spooner, 2002), and the latter was interpreted as magmatic water (Samson & Russell, 1987), metamorphic water (Russell, 1973; Phillips, 1983) and/or deep circulating seawater (Russell, 1978; Samson & Russell, 1987). Based on fluid inclusion and H–O isotope studies (Yang *et al.* 2018; Wang *et al.*, 2021, the ore-forming fluids of the Tianbaoshan deposit are characterized by a large range

in temperature (87–273 °C) and salinity (3–22 wt % NaCl equiv.), which was mainly sourced from basinal brine with the addition of metamorphic water.

The mechanism of sulphide mineral precipitation could be constrained by the origin of H<sub>2</sub>S in the mixing model. The reduced sulphur is derived from thermochemical sulphate reduction (TSR) and/or from bacterial sulphate reduction (BSR) (Ghazban *et al.* 1990). The available temperature range for BSR is 30 to 45 °C (Orr, 1974), and the upper limit is 84 °C (Trudinger *et al.* 1985). There is no doubt that the conditions for BSR are not suitable at elevated temperatures (78–198 °C) for sulphide deposition

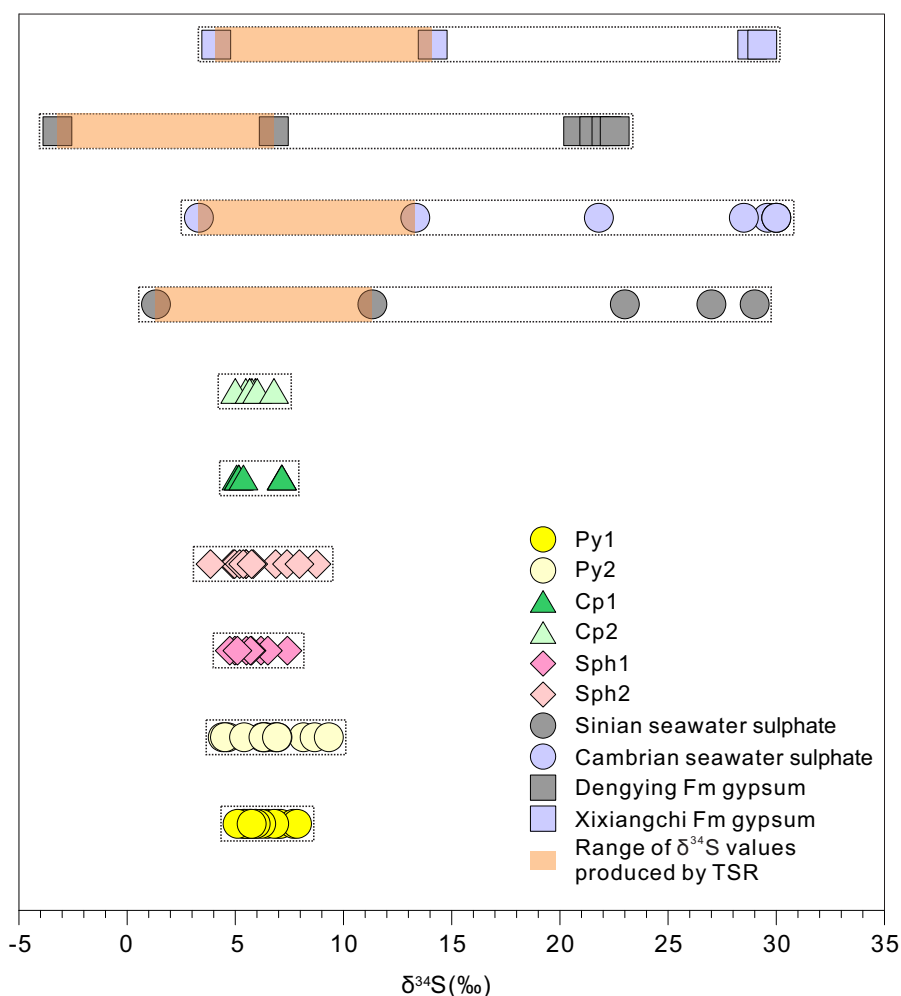
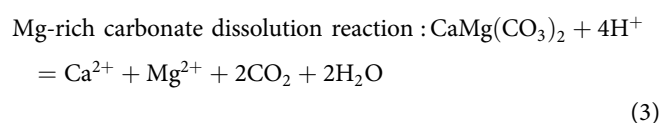
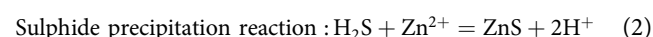
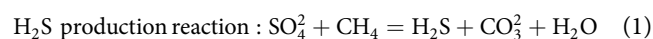


**Fig. 11.** (Colour online) Sulphur isotopes of different types of pyrites (Py1 and Py2), chalcopyrites (Cp1 and Cp2) and sphalerites (Sph1 and Sph2) by LA-MC-ICP-MS in comparison with typical  $\delta^{34}\text{S}$  values for gypsum in Dengying and Xixiangchi Formations (Zhu *et al.* 2006) and Cambrian and Sinian seawater sulphate (Canfield & Farquhar, 2009).

at Tianbaoshan. In terms of identifying the sulphur source (e.g. seawater sulphate or gypsum), the range in sulphur isotope fractionation caused by BSR is larger than the isotope fractionation of 15–25 ‰ obtained by TSR (Ohmoto & Goldhaber, 1997). At Tianbaoshan, the  $\delta^{34}\text{S}$  values of all sulphide minerals (3.9 to 9.3 ‰) fall within the range of  $\delta^{34}\text{S}$  values produced by TSR (Fig. 11). Therefore, it is most likely that the mixing model involving thermochemical sulphate reduction is the main mechanism for Tianbaoshan ore formation.

Support for this mechanism comes from the tube-like shape of the main orebody (Figs 2, 3a–b) which is compatible with the deposit filling a void that was produced by dissolution of the host dolomite. In addition, a large number of dissolved structures are observed in the Tianbaoshan deposit, e.g. caverns and breccias (Fig. 5). The host rock remnants are suspended within the massive ore (Fig. 5a–b), and many sulphides grow around host rock breccias in brecciated ore (Fig. 5c, e–f) where the host rock fragments exhibit deformation structures. These physical features indicate that replacement of the host dolostones by ore fluids is volumetrically significant and the ore was formed simultaneously with the cavity which it fills. Moreover, some cavities are also present in the massive sulphide ore and are filled with calcite (Fig. 5a–b, d, f), indicating that calcite formation postdates sulphide mineralization. The processes in this model can be expressed as three reactions:



Based on this model,  $\text{H}_2\text{S}$  from Eq. 1 can generate acid by precipitating sulphide (Eq. 2). This, in turn, may cause dissolution and brecciation of adjacent carbonate rocks (Eq. 3). Thus, dissolution and brecciation could occur at the same time as mineralization. Although carbonate and sulphide cannot precipitate together, the association of sulphide minerals (e.g. pyrite, sphalerite and galena) and quartz (Figs 6a–d, 7e–f) indicates that silicification occurred in the host rock during sulphide mineralization (Anderson & Garven, 1987).

There are two mechanisms of sulphate reduction in the mixing model. One is that sulphate-bearing fluid encountered hydrocarbon within the flow path and produced  $\text{H}_2\text{S}$ -bearing fluid that was carried to a mixing site with the introduction of metal-bearing fluid (Ghazban *et al.* 1990; Plumlee *et al.* 1994). Alternatively, both the sulphate-bearing fluid and metal-bearing fluid arrived at the mixing site which already contained the reducing agent

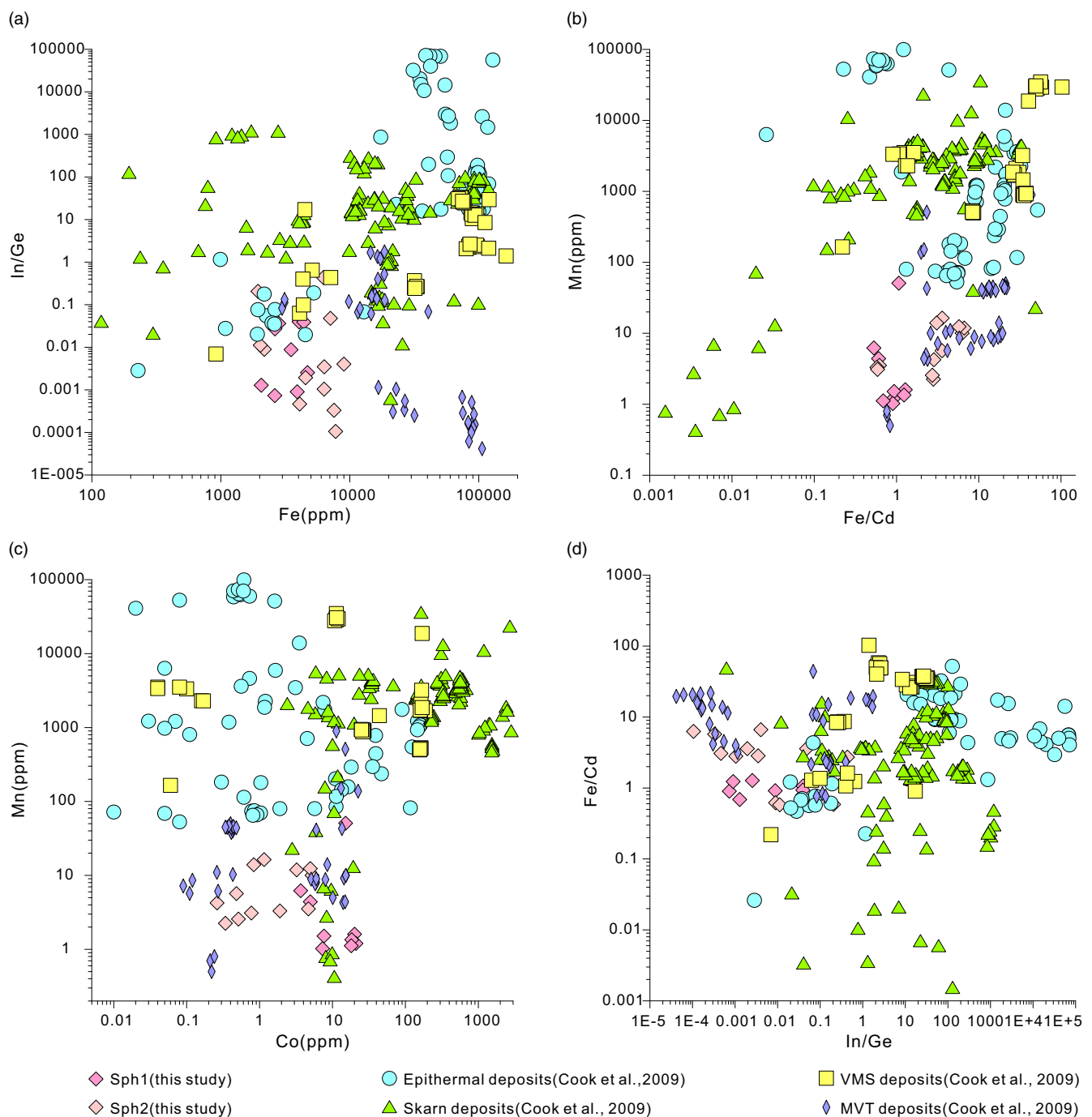


**Fig. 12.** (Colour online) Binary plots of Fe vs In/Ge (a), Fe/Cd vs Mn (b), Co vs Mn (c) and In/Ge vs Fe/Cd (d) for sphalerite at Tianbaoshan compared with epithermal, VMS, skarn and MVT-type Pb-Zn deposits. Data from Cook *et al.* (2009).

(e.g. hydrocarbon) (Crocetti & Holland, 1989; Leventhal, 1990; Anderson, 1991). However, the eventual reaction is interaction between a H<sub>2</sub>S-bearing fluid and a metal-bearing fluid at the deposition site (e.g. carbonate host rock). These processes can be constrained by studying the components of the ore-forming fluids. Most data from fluid inclusions in sphalerite (Yu *et al.* 2015; Wang *et al.*, 2021; Yang *et al.* 2018) indicate that the vapour phase was mainly composed of H<sub>2</sub>O and CO<sub>2</sub>, with only minor reduced species (e.g. CH<sub>4</sub>). In addition, reducing materials (e.g. bitumen) are not observed in the hand specimens (Fig. 5). Therefore, it is

most likely that sulphate reduction took place before ore precipitation rather than during ore precipitation. Evaporite (e.g. gypsum) from the Sinian Dengying Formation and Cambrian Xixiangchi Formation (Zhu *et al.* 2006) provides an important source for generating reduced sulphur. Based on the characteristics discussed above, we suggest that regional groundwater flowed through evaporate-rich strata and encountered sulphate reduction to form H<sub>2</sub>S-rich fluid, mixed with metal-rich fluid ascending through the fault at the deposition site, and eventually caused massive sulphide mineralization together with significant carbonate dissolution.

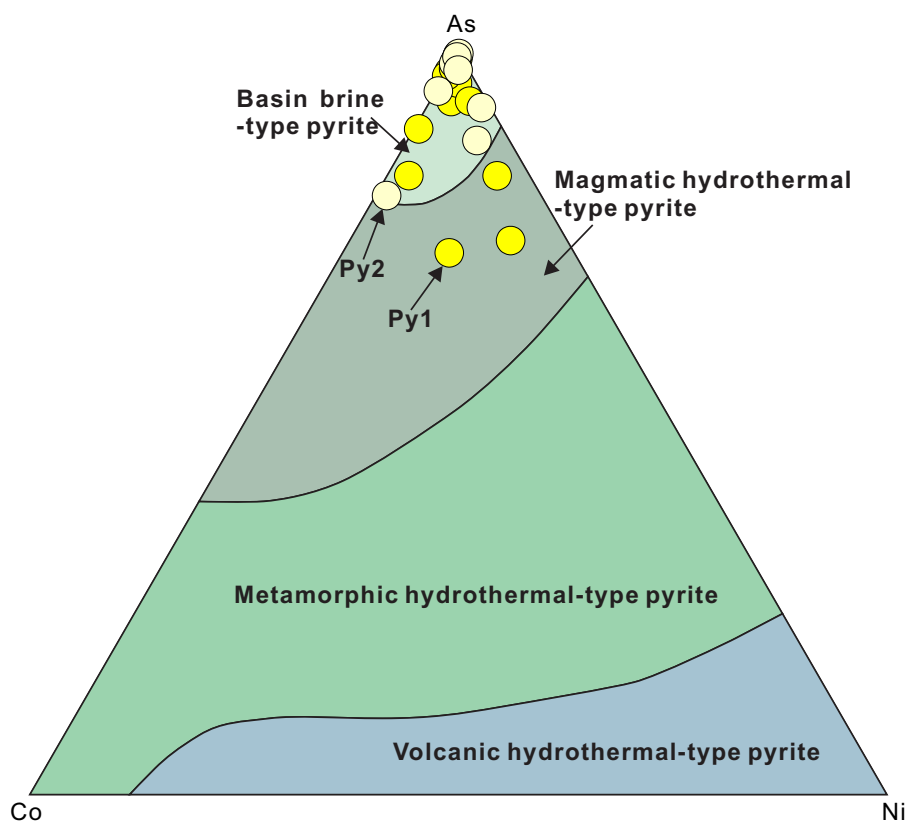


**Fig. 13.** (Colour online) Plot showing Co–Ni–As content variation of pyrite in Tianbaoshan deposit (modified from Gong & Ma, 2011).

These data and interpretations are important for Pb–Zn–Cu exploration in the Tianbaoshan ore district. An exploration model should focus on: (1) the combining studies of specific structures and alteration in the host rock, especially extensive dissolved structures (caverns and breccias) and prominent silicification assemblages; and (2) developing a quantitative index of the sulphides, namely a uniform sulphur isotope signature and an intermediate-to low-temperature feature of characteristic trace elements (e.g. Mn, In, Ge and Cd), which can be used for providing geochemical tools or index systems to identify and exploit deposits.

## 7. Conclusions

- (1) Sulphides from the Tianbaoshan deposit, consisting of pyrite, chalcopyrite, sphalerite and galena, are typically contained within space-filling structures (massive and brecciated) and textures (relic texture, poikilitic texture, caverns and fracture-filling veins). These textural relationships reveal that the sulphide minerals underwent four paragenetic stages: early stage (Py1) of pyrite relics (Stage 1); early stage (Cp1) of coarse-grained, elliptical crystal chalcopyrite (Stage 2); main stage of dark-coloured, fine-grained sphalerite (Sph1) and light-coloured, coarse-grained sphalerite (Sph2) (Stage 3); and late stage (Py2, Cp2 and Gn) of sulphide veinlets (Stage 4).
- (2) Textures in the main sulphides including Py1, Cp1, Sph1 and Sph2 demonstrate mutual inclusion relationships from core to rim and they have nearly uniform sulphur isotope signatures (5.5–8.3 ‰), which is the result of different stages of mineralization throughout a continuous hydrothermal system.
- (3) The Tianbaoshan deposit resembles a typical MVT-type deposit, with dolostone host rock, open space filling and a

weak alteration style. Sphalerite and chalcopyrite geothermometer studies indicate that the ore-forming fluid was an intermediate- to low-temperature (< 200 °C) hydrothermal system. The low contents of Mn and In, low In/Ge ratios and high Fe/Cd ratios in sphalerites, and high S/Fe mole ratios, low Se contents and high S/Se ratios in pyrites are consistent with those of MVT deposits but are different than those of magmatism-related deposits (i.e. epithermal, skarn and VMS deposits).

- (4) The Tianbaoshan deposit developed extensive dissolved structures (caverns and breccias) with massive sulphide infillings and deformed host rock remnants, suggesting that replacement of the host dolostones by ore fluids was volumetrically significant and the ore formed simultaneously with the cavity formation. Both carbonate dissolution and sulphide formation can be attributed to mixing between a H<sub>2</sub>S-rich fluid and a metal-rich fluid with thermochemical sulphate reduction occurring before ore precipitation rather than during ore precipitation.

**Supplementary material.** To view supplementary material for this article, please visit <https://doi.org/10.1017/S0016756822001054>

**Acknowledgements.** We are greatly indebted to Senior Engineer Shun-Ping Qin (Sichuan Huili Zinc & Plumbum Company Limited) for the assistance during fieldwork. This research was supported by the opening funding of State Key Laboratory of Ore Deposit Geochemistry, Institute of Geochemistry, Chinese Academy of Sciences (Grant No. 202008), the Science and Technology Project of Sichuan Province (No. 2022YFS0451), and the Science and technology Project of Tibet Autonomous Region (No. XZ202102YD0024C, XZ201801-GB-01).



## References

- Abidi R, Slim-Shimi N, Somarin A and Henchiri M** (2010) Mineralogy and fluid inclusions study of carbonate-hosted Mississippi valley-type Ain Allega Pb–Zn–Sr–Ba ore deposit, Northern Tunisia. *Journal of African Earth Sciences* **57**, 262–72.
- Anderson GM** (1991) Organic maturation and ore precipitation in Southeast Missouri. *Economic Geology* **86**, 909–26.
- Anderson GM and Garven G** (1987) Sulfate-sulfide-carbonate associations in Mississippi Valley-type lead-zinc deposits. *Economic Geology* **82**, 482–8.
- Ashton J, Boyce A, Fallick A and Russell M** (1998) Ore depositional process in the Navan Zn–Pb deposit, Ireland. *Economic Geology* **93**, 535–63.
- Banks DA and Russell MJ** (1992) Fluid mixing during ore deposition at the Tynagh base metal deposit, Ireland. *European Journal of Mineralogy* **4**, 921–31.
- Barrie CD, Boyce AJ, Boyle AP, Williams PJ, Blake K, Wilkinson JJ, Lowther M, McDermott P and Prior DJ** (2009) On the growth of colloform textures: a case study of sphalerite from the Galmoy orebody, Ireland. *Journal of the Geological Society* **166**, 563–82.
- Basuki NI and Spooner ETC** (2002) A review of fluid inclusion temperatures and salinities in Mississippi Valley-type Zn–Pb deposits: Identifying thresholds for metal transport. *Exploration and Mining Geology* **11**, 1–17.
- Blakeman RJ, Ashton JH, Boyce AJ, Fallick AE and Russell MJ** (2002) Timing of interplay between hydrothermal and surface fluids in the Navan Zn+Pb orebody, Ireland: evidence from metal distribution trends, mineral textures and  $\delta^{34}\text{S}$  analyses. *Economic Geology* **97**, 73–91.
- Bouabdellah M, Boudchiche L, Ouahhabi B and Naciri T** (2008) Origin of sulfur associated to the eastern Beni Snassen Pb–Zn Mississippi Valley-type deposits (northeastern Morocco). *C.R. Geoscience* **340**, 822–8.
- Bouabdellah M, Sangster DF, Leach DL, Brown AC, Johnson CA and Emso AP** (2012) Genesis of the Touissit-Bou Beker Mississippi Valley-type district (Morocco-Algeria) and its relationship to the Africa-Europe collision. *Economic Geology* **107**, 117–46.
- Cai LM** (2012) Study on the ore-controlling structures in Tianbaoshan Pb–Zn deposit, Huili, Sichuan. Dissertation, Chengdu University of Technology (in Chinese with English abstract).
- Canfield DE and Farquhar J** (2009) Animal evolution, bioturbation, and the sulfate concentration of the oceans. *Proceedings of the National Academy of Sciences of the USA* **106**, 8123–8127.
- Cave B, Lilly R and Barovich K** (2020) Textural and geochemical analysis of chalcopyrite, galena and sphalerite across the Mount Isa Cu to Pb–Zn transition: implications for a zoned Cu–Pb–Zn system. *Ore Geology Reviews* **124**. doi:10.1016/j.oregeorev.2020.103647.
- Chen SJ** (1986) Research on the genesis of lead–zinc ore deposit in western Guizhou and northeastern Yunnan. *Guizhou Geology* **3**, 211–22 (in Chinese with English abstract).
- Cheng HZ** (2013) A research and a prospecting practice on the fault structure in Tianbaoshan lead–zinc mine, Huili, Sichuan. *Mineral Resources and Geology* **27**, 298–302 (in Chinese with English abstract).
- Cook NJ, Ciobanu CL, Pring A, Skinner W, Shimizu M, Danyushevsky L, Saini-Eidukat B and Melcher F** (2009) Trace and minor elements in sphalerite: a LA-ICPMS study. *Geochimica et Cosmochimica Acta* **73**, 4761–91.
- Corbella M, Ayora C and Cardellach E** (2004) Hydrothermal mixing, carbonate dissolution and sulfide precipitation in Mississippi Valley-type deposits. *Mineralium Deposita* **39**, 344–57.
- Coveney Jr. RM, Goebel ED and Ragan VM** (1987) Pressures and temperatures from aqueous fluid inclusions in sphalerite from midcontinent country rocks. *Economic Geology* **82**, 740–751.
- Crocetti CA and Holland HD** (1989) Sulfur-lead isotope systematics and the composition of fluid inclusions in galena from the Viburnum Trend, Missouri. *Economic Geology* **84**, 2196–216.
- Deloule E, Allegre C and Doe B** (1986) Lead and sulfur isotope microstratigraphy in galena crystals from Mississippi Valley type deposits. *Economic Geology* **81**, 1307–21.
- Elliott HAL, Gernon TM, Roberts S, Boyce AJ and Hewson C** (2019) Diatremes act as fluid conduits for Zn–Pb mineralization in the SW Irish ore field. *Economic Geology* **114**, 117–25.
- Everett CE, Wilkinson JJ and Rye DM** (1999) Fracture controlled fluid flow in the Lower Palaeozoic basement rocks of Ireland: implications for the genesis of Irish-type Zn–Pb deposits. In *Fractures, Fluid Flow and Mineralisation* (eds KJW McCaffrey, L Lonergan and JJ Wilkinson), pp. 247–76. Geological Society of London, Special Publication no. 155.
- Eyre SL** (1998) *Geochemistry of dolomitization and Zn–Pb mineralization in the Rathdowney Trend, Ireland*. Unpublished PhD thesis, University of London, 414p.
- Fazli S, Taghipour B, Moore F and Lentz DR** (2019) Fluid inclusions, S isotopes, and Pb isotopes characteristics of the Kuh-e-Surmeh carbonate-hosted Zn–Pb deposit in the Zagros Fold Belt, southwest Iran: implications for the source of metals and sulfur and MVT genetic model. *Ore Geology Reviews* **109**, 615–29.
- Feng JQ, Li Y and Liu WZ** (2009) Geological features and ore control conditions for the Tianbaoshan Pb–Zn deposit in Huili. *Acta Geologica Sichuan* **29**, 426–30, 434 (in Chinese with English abstract).
- Ferrini V, Fayek M, De Vito C, Mignardi S and Pignatti J** (2010) Extreme sulphur isotope fractionation in the deep Cretaceous biosphere. *Journal of the Geological Society* **167**, 1009–18.
- Frenzel M, Hirsch T, Gutzmer J** (2016) Gallium, germanium, indium, and other trace and minor elements in sphalerite as a function of deposit type – A meta-analysis. *Ore Geology Reviews* **76**, 52–78.
- Gagnevin D, Menuge JF, Kronz A, Barrie C and Boyce AJ** (2014) Minor elements in layered sphalerite as a record of fluid origin, mixing, and crystallization in the Navan Zn–Pb ore deposit, Ireland. *Economic Geology* **109**, 1513–28.
- Ghazban F, Schwarcz HP and Ford DC** (1990) Carbon and sulfur isotope evidence for in situ reduction of sulfate, Nanisivik lead–zinc deposits, Northwestern Territories, Baffin Island, Canada. *Economic Geology* **85**, 360–75.
- Gong L and Ma G** (2011) The characteristic typomorphic composition of pyrite and its indicative meaning to metal deposits. *Contributions to Geology and Mineral Resources Research* **26**, 162–6 (in Chinese with English abstract).
- Han RS, Liu CQ, Huang ZL, Chen J, Ma DY, Lei L and Ma GS** (2007) Geological features and origin of the Huize carbonate-hosted Zn–Pb–(Ag) district, Yunnan, South China. *Ore Geology Reviews* **31**, 360–83.
- Horn S, Dziggel A, Kolb J and Sindern S** (2019) Textural characteristics and trace element distribution in carbonate-hosted Zn–Pb–Ag ores at the Paleoproterozoic Black Angel deposit, central West Greenland. *Mineralium Deposita* **54**, 507–24.
- Hu RZ and Zhou MF** (2012) Multiple Mesozoic mineralization events in South China: an introduction to the thematic issue. *Mineralium Deposita* **47**, 579–88.
- Hu YS, Ye L, Li ZL, Huang ZL and Zhang JW** (2018) Genesis of fahlore in the Tianbaoshan lead–zinc deposit, Sichuan Province, China: a scanning electron microscopy–energy dispersive spectroscopy study. *Acta Geochimica* **37**, 842–53.
- Kesler SE, Appold MS, Martini AM, Walter LM, Huston TJ and Kyle JR** (1995) Na–Cl–Br systematics of mineralizing brines in Mississippi Valley-type deposits. *Geology* **23**, 641–4.
- Knorsch M, Nadoll P and Klemm R** (2020) Trace elements and textures of hydrothermal sphalerite and pyrite in Upper Permian (Zechstein) carbonates of the North German Basin. *Journal of Geochemical Exploration* **209**. doi:10.1016/j.gexplo.2019.106416.
- Layne GD, Hart SR and Shimizu N** (1991) Microscale lead and sulfur isotope zonation in hydrothermal sulfides by ion microprobe: new findings from the Mississippi Valley-type Pb–Zn deposits of the Viburnum Trend, S.E. Missouri. *Geological Society of America Abstracts with Program* **23**, 101–2.
- Leach DL** (1979) Temperature and salinity of the fluids responsible for minor occurrences of sphalerite in the Ozark region of Missouri. *Economic Geology* **74**, 931–937.
- Leach DL, Sangster DF, Kelley KD, Large RR, Garven G, Allen CR, Gutzmer J and Walters S** (2005) Sediment-hosted lead–zinc deposits: a global perspective. In *Economic Geology 100th Anniversary*, Society of Economic Geologists. pp. 561–608.
- Leach DL, Taylor RD, Fey DL, Diehl SF and Saltus RW** (2010) A deposit model for Mississippi Valley-type lead–zinc ores. Chapter A of mineral

- deposit models for resource assessment. *USGS, Scientific Investigations Report 5070-A*. Reston, VA: US Geological Survey.
- Leng CB, Wang W, Ye L and Zhang XC** (2018) Genesis of the late Ordovician Kukaazi Pb–Zn deposit in the western Kunlun orogen, NW China: new insights from in-situ trace elemental compositions of base metal sulfides. *Journal of Asian Earth Sciences* **184**. doi:10.1016/j.jseaes.2019.103995.
- Leventhal JS** (1990) Organic matter and thermochemical sulfate reduction in the Viburnum Trend, southeast Missouri. *Economic Geology* **85**, 622–32.
- Li B, Zhou JX, Huang ZL, Yan ZF, Bao GP and Sun HR** (2015) Geological, rare earth elemental and isotopic constraints on the origin of the Banbanqiao Zn–Pb deposit, southwest China. *Journal of Asian Earth Sciences* **111**, 100–12.
- Li HM, Mao JM, Zhang CQ, Xu H and Chen YC** (2004) The composition, texture and origin of organic matter in basalt-type copper deposits in the northeastern Yunnan–Western Guizhou area. *Acta Geologica Sinica* **78**, 519–26 (in Chinese with English abstract).
- Li ZL, Ye L, Hu YS and Huang ZL** (2018) Geological significance of nickeliferous minerals in the Fule Pb–Zn deposit, Yunnan Province, China. *Acta Geochimica* **37**, 684–90.
- Liu HC and Lin WD** (1999) *Study on the Law of Pb–Zn–Ag Ore Deposit in Northeast Yunnan*. Kunming: Yunnan University Press, 468 pp. (in Chinese).
- Liu YS, Hu ZC, Gao S, Günther D, Xu J, Gao CG and Chen HL** (2008) In situ analysis of major and trace elements of anhydrous minerals by LA–ICP–MS without applying an internal standard. *Chemical Geology* **257**, 34–43.
- Maul B** (1991) *Vom vadosen Bereich zur Anchimetamorphose. Diagenese des Oberen Wettersteinkalks der westlichen Nördlichen Kalkalpen*. Doctoral Thesis, Albert-Ludwigs University, Freiburg.
- Maurer M, Prelević D, Mertz-Kraus R, Pačevski A, Kostić B and Malbašić J** (2019) Genesis and metallogenetic setting of the polymetallic barite sulphide deposit, Bobija, Western Serbia. *International Journal of Earth Sciences* **108**, 1725–40.
- Mazzullo SJ and Harris PM** (1992) Mesogenetic dissolution: its role in porosity development in carbonate reservoirs. *American Association of Petroleum Geologists Bulletin* **76**, 607–20.
- McKibben MA and Eldridge CS** (1995) Microscopic sulfur isotope variations in ore minerals from the Viburnum Trend, Southeast Missouri: a SHRIMP study. *Economic Geology* **90**, 228–45.
- Muhling JR, Fletcher IR and Rasmussen B** (2012) Dating fluid flow and Mississippi Valley type base-metal mineralization in the Paleoproterozoic Earraheedy Basin, Western Australia. *Precambrian Research* **212–213**, 75–90.
- Niroomand S, Hagi A, Rajabi A, Shabani AAT and Song YC** (2019) Geology, isotope geochemistry, and fluid inclusion investigation of the Robat Zn–Pb–Ba deposit, Malayer–Esfahan metallogenic belt, southwestern Iran. *Ore Geology Reviews* **112**. doi:10.1016/j.oregeorev.2019.103040.
- Ohmoto H and Goldhaber MB** (1997) Sulfur and carbon isotopes. In *Geochemistry of Hydrothermal Ore Deposits*, 3rd edn (ed. HL Barnes), pp. 517–612. New York: Wiley.
- Orr WL** (1974) Changes in sulfur content and isotopic ratios of sulfur during petroleum maturation–study of Big Horn basin Paleozoic oils. *American Association of Petroleum Geologists Bulletin* **58**, 2295–18.
- Oyebamiji A, Hu RZ, Zhao CH and Zafar T** (2020) Origin of the Triassic Qilinchang Pb–Zn deposit in the western Yangtze block, SW China: insights from in-situ trace elemental compositions of base metal sulphides. *Journal of Asian Earth Sciences* **192**. doi:10.1016/j.jseaes.2020.104292.
- Peever J, Fayek M, Misra KC and Riciputi LR** (2003) Sulfur isotope micro-analysis of sphalerite by SIMS: constraints on the genesis of Mississippi Valley-type mineralization, from the Mascot–Jefferson City district, East Tennessee. *Journal of Geochemical Exploration* **80**, 277–96.
- Perona J, Canals A and Cardellach E** (2018) Zn–Pb mineralization associated with salt diapirs in the Basque–Cantabrian Basin, Northern Spain: Geology, Geochemistry, and Genetic Model. *Economic Geology* **113**, 1133–1159.
- Pfaff KT, Wagner T and Markl G** (2009) Fluid mixing recorded by mineral assemblage and mineral chemistry in a Mississippi Valley–type Pb–Zn–Ag deposit in Wiesloch, SW Germany. *Journal of Geochemical Exploration* **101**, 81.
- Phillips WJ** (1983) Discussion of Boyce et al. (1983). *Transactions of Institution of Mining and Metallurgy* **92**, B102.
- Plumlee GS, Leach DL, Hofstra AH, Landis GP, Rowan EL and Viets JG** (1994) Chemical reaction path modeling of ore deposition in Mississippi valley–type Pb–Zn deposits of the Ozark region, U.S. Midcontinent. *Economic Geology* **89**, 1361–83.
- Qing H and Mountjoy EW** (1994) Origin of dissolution vugs, caverns and breccias in the middle Devonian Presqu’île Barrier, host of Pine Point MVT deposits. *Economic Geology* **89**, 858–76.
- Russell MJ** (1978) Downward-excavating hydrothermal cells and Irish-type ore deposits: importance of an underlying thick Caledonian prism. *Transactions of Institution of Mining and Metallurgy* **87**, B168–71.
- Russell MJ** (1973) Base-metal mineralization in Ireland and Scotland and the formation of Rockall Trough. In *Implications of Continental Drift to the Earth Sciences*, vol. 1 (eds DH Tarling and SK Runcorn), pp. 581–97. London: Academic.
- Saintilan NJ, Stephens MB, Lundstam E and Fontboté L** (2015) Control of reactivated Proterozoic basement structures on sandstone-hosted Pb–Zn deposits along the Caledonian Front, Sweden: evidence from airborne magnetic data, structural analysis, and ore-grade modeling. *Economic Geology* **110**, 91–117.
- Samson IM and Russell MJ** (1987) Genesis of the silvermines zinc–lead–barite deposit, Ireland: fluid inclusion and stable isotope evidence. *Economic Geology* **82**, 371–94.
- Sangster DF** (1990) Mississippi Valley-type and sedex lead–zinc deposits: a comparative examination. *Transactions – Institution of Mining and Metallurgy. Section B. Applied Earth Science* **99**, 21–42.
- Shelton KL, Bauer RM and Gregg JM** (1992) Fluid inclusion studies of regionally extensive epigenetic dolomites, Bonnetterre Dolomite (Cambrian), southeast Missouri: Evidence of multiple fluids during dolomitization and lead–zinc mineralization. *Geological Society of America Bulletin* **104**, 675–683.
- Sun HR, Zhou JX, Huang ZL, Fan HF, Ye L, Luo K and Gao JG** (2016) The genetic relationship between Cu and Zn dominant mineralization in the Tianbaoshan deposit, Southwest China. *Acta Petrologica Sinica* **32**, 3407–17 (in Chinese with English abstract).
- Sverjensky DA** (1986) Genesis of Mississippi Valley–type lead–zinc deposits. *Annual Review of Earth and Planetary Sciences* **14**, 177–99.
- Symons DTA, Lewchuk MT, Kawasaki K, Velasco F and Leach DL** (2009) The Reocin zinc–lead deposit, Spain: paleomagnetic dating of a late Tertiary ore body. *Mineralium Deposita* **44**, 867–80.
- Tan SC, Zhou JX, Zhou MF and Ye L** (2019) In-situ S and Pb isotope constraints on an evolving hydrothermal system, Tianbaoshan Pb–Zn–(Cu) deposit in South China. *Ore Geology Reviews* **115**. doi:10.1016/j.oregeorev.2019.103177.
- Trudinger PA, Chambers LA and Smith JW** (1985) Low temperature sulfate reduction: biological versus abiological. *Canadian Journal of Earth Sciences* **22**, 1910–18.
- Tu GC** (2002) Two unique mineralization areas in Southwest China. *Bulletin of Mineralogy, Petrology and Geochemistry* **21**, 1–2 (in Chinese with English abstract).
- Tu GZ** (1984) *Geochemistry of Strata-bound Ore Deposits in China (Volume I)*. Beijing: Science Press, pp. 13–69 (in Chinese with English abstract).
- Wang H, Zhu XY, Wang JB, Jia DL, Shi Y, Chen L and Xu ZF** (2021). Sources of metallogenic materials and metallogenic mechanism of Tianbaoshan Pb–Zn deposit in Sichuan Province: Constraints from fluid inclusions and isotopic evidences. *Acta Petrologica Sinica*, **37**, 1830–1846 (in Chinese with English abstract).
- Wang J, Zhang J, Zhong WB, Yang Q, Li F and Zhu ZK** (2018) Sources of ore-forming fluids from Tianbaoshan and Huize Pb–Zn deposits in Yunnan–Sichuan–Guizhou region, southwest China: evidence from fluid inclusions and He–Ar isotopes. *Earth Science* **43**, 2076–99.
- Wang XC** (1992) Genesis analysis of the Tianbaoshan Pb–Zn deposit. *Journal of Chengdu College of Geology* **19**, 10–20 (in Chinese with English abstract).
- Wang XC, Zhang ZR, Zheng MH and Xu XH** (2000) Metallogenic mechanism of the Tianbaoshan Pb–Zn deposit, Sichuan. *Chinese Journal of Geochemistry* **19**, 121–33.

- Wang XG, Li R, Cai LP and Yang J (2010) Geological features, ore-forming conditions and prospecting potential of the Emeishan basalt-hosted Cu deposits in the Sichuan–Yunnan–Guizhou Border Region. *Acta Geologica Sichuan* **30**, 174–82 (in Chinese with English abstract).
- Wang YG and Wang SY (2003) Emeishan large igneous provinces and basalt copper deposits: an example from Permian basalt areas in Guizhou. *Guizhou Geology* **20**, 5–10, 4 (in Chinese with English abstract).
- Wei AY, Xue CD, Xiang K, Li J, Liao C and Akhter QJ (2015) The ore-forming process of the Maoping Pb–Zn deposit, northeastern Yunnan, China: constraints from cathodoluminescence (CL) petrography of hydrothermal dolomite. *Ore Geology Reviews* **70**, 562–77.
- Wilkinson JJ, Eyre SL and Boyce AJ (2005) Ore-forming processes in Irish-type carbonate-hosted Zn–Pb deposits: evidence from mineralogy, chemistry, and isotopic composition of sulfides at the Lisheen mine. *Economic Geology* **100**, 63–86.
- Wu Y (2013) *The age and ore-forming process of MVT deposits in the boundary area of Sichuan–Yunnan–Guizhou provinces, Southwest China*. PhD thesis, China University of Geosciences, Beijing, 167 pp. (in Chinese with English abstract).
- Wu Y, Zhang CQ, Mao JW, Ouyang HG and Sun J (2013) The genetic relationship between hydrocarbon systems and Mississippi Valley–type Zn–Pb deposits along the SW margin of Sichuan Basin, China. *Int Geol Rev* **55**, 941–957.
- Xiao CH and Li GJ (2019) Geological, sulfur isotopic, and mineral trace element constraints on the genesis of the Xiyi Pb–Zn deposit, Baoshan Block, SW China. *Journal of Asian Earth Sciences* **186**, doi:10.1016/j.jseaes.2019.104056.
- Xiong SF, Gong YJ, Jiang SY, Zhang XJ, Li Q and Zeng GP (2018) Ore genesis of the Wusihe carbonate-hosted Zn–Pb deposit in the Dadu River Valley district, Yangtze Block, SW China. *Mineralium Deposita* **53**, 967–979.
- Xu Y, Huang Z, Zhu D and Luo T (2014) Origin of hydrothermal deposits related to the Emeishan magmatism. *Ore Geology Reviews* **63**, 1–8.
- Yang Q, Zhang J, Wang J, Zhong WB and Liu WH (2018) Ore-forming fluid and isotope geochemistry of Tianbaoshan large carbonate hosted Pb–Zn deposit in Sichuan Province. *Mineral Deposits* **37**, 816–34 (in Chinese with English abstract).
- Ye L, Cook NJ, Ciobanu CL, Liu Y, Zhang Q, Liu TG, Gao W, Yang YL and Danyushevsky L (2011) Trace and minor elements in sphalerite from base metal deposits in South China: a LA–ICPMS study. *Ore Geology Reviews* **39**, 188–217.
- Ye L, Li ZL, Hu YS, Huang ZL, Zhou JX, Fang HF and Danyushevskiy L (2016) Trace elements in sulfide from the Tianbaoshan Pb–Zn deposit, Sichuan Province, China: a LA–ICPMS study. *Acta Petrologica Sinica* **32**, 3377–93 (in Chinese with English abstract).
- Yu C, Wei ML and Hu GC (2015) The geochemical feature of fluid inclusion in Tianbaoshan Pb–Zn deposit of Huili, Sichuan. *Yunnan Geology* **34**, 531–8 (in Chinese with English abstract).
- Yuan B, Zhang C, Yu H, Yang Y, Zhao Y, Zhu C, Ding Q, Zhou Y, Yang J and Xu Y (2018) Element enrichment characteristics: insights from element geochemistry of sphalerite in Daliangzi Pb–Zn deposit, Sichuan, Southwest China. *Journal of Geochemical Exploration* **186**, 187–201.
- Zhang CQ (2008) *The genetic model of Mississippi Valley–type deposits in the boundary area of Sichuan, Yunnan and Guizhou Province, China*. PhD dissertation, Chinese Academy of Geological Sciences, Beijing, 177 pp. (in Chinese with English abstract).
- Zhang CQ, Mao JW, Wu SP, Li HM, Liu F, Guo BJ and Gao DR (2005) Distribution, characteristics and genesis of Mississippi Valley–Type lead zinc deposit in Sichuan–Yunnan–Guizhou area. *Mineral Deposits* **24**, 336–48 (in Chinese with English abstract).
- Zhang CQ, Wu Y, Hou L and Mao JW (2015a) Geodynamic setting of mineralization of Mississippi Valley–type deposits in world-class Sichuan–Yunnan–Guizhou Zn–Pb triangle, southwest China: implications from age-dating studies in the past decade and the Sm–Nd age of Jinshachang deposit. *Journal of Asian Earth Sciences* **103**, 103–14.
- Zhang F (2017) *Study on ore genesis of the Tianbaoshan Pb–Zn deposit and the regional metallogenetic geodynamical setting*. Master's thesis, China University of Geosciences (Beijing), 73 pp. (in Chinese with English abstract).
- Zhang HJ, Fan HF, Xiao CY, Wen HJ, Ye L, Huang ZL, Zhou JX and Guo QJ (2019a) The mixing of multi-source fluids in the Wusihe Zn–Pb ore deposit in Sichuan Province, Southwestern China. *Acta Geochim* **38**, 642–653.
- Zhang HJ, Xiao CY, Wen HJ, Zhu XK, Ye L, Huang ZL, Zhou JX and Fan HF (2019b) Homogeneous Zn isotopic compositions in the Maozu Zn–Pb ore deposit in Yunnan Province, southwestern China. *Ore Geology Reviews* **109**, 1–10.
- Zhang LJ, Qin MF, Zeng WL, Li DS, Zeng NS, Ruan QF, Song CX and Hu HY (2015b) Mineralogy and genesis of bitumen and Cu-bearing minerals in amygdaloid basalt from southern Sichuan Province, China. *Acta Mineralogica Sinica* **35**, 127–35 (in Chinese with English abstract).
- Zhang ZB, Li CY, Tu GC, Xia B and Wei ZQ (2006) Geotectonic evolution background and ore-forming process of Pb–Zn deposits in Chuan–Dian–Qian area of southwest China. *Geotectonica et Metallogenia* **30**, 343–354 (in Chinese with English abstract).
- Zhou CX, Wei CS and Guo JY (2001) The source of metals in the Qilingchang Pb–Zn deposit, Northeastern Yunnan, China: Pb–Sr isotope constraints. *Economic Geology* **96**, 583–98.
- Zhou JX, Gao JG, Chen D and Liu XK (2013) Ore genesis of the Tianbaoshan carbonate hosted Pb–Zn deposit, Southwest China: geologic and isotopic (C–H–O–S–Pb) evidence. *International Geology Review* **55**, 1300–10.
- Zhou JX, Huang ZL, Zhou MF, Zhu XK and Muchez P (2014) Zinc, sulfur and lead isotopic variations in carbonate-hosted Pb–Zn sulfide deposits, southwest China. *Ore Geology Reviews* **58**, 41–54.
- Zhou JX, Xiang ZZ, Zhou MF, Feng YX, Luo K, Huang ZL and Wu T (2018) The giant Upper Yangtze Pb–Zn province in SW China: reviews, new advances and a new genetic model. *Journal of Asian Earth Sciences* **154**, 280–315.
- Zhu CW, Wen HJ, Zhang YX, Fan HF (2016) Cadmium and sulfur isotopic compositions of the Tianbaoshan Zn–Pb–Cd deposit, Sichuan Province, China. *Ore Geology Reviews* **76**, 152–162.
- Zhu CW, Wen HJ, Zhang YX, Fu SH, Fan HF and Cloquet C (2017) Cadmium isotope fractionation in the Fule Mississippi Valley type deposit, Southwest China. *Mineralium Deposita* **52**, 675–86.
- Zhu GY, Zhang SC, Liang YB and Li QR (2006) The formation of H<sub>2</sub>S and its evidence of Weiyuan large gas field in Sichuan basin. *Chinese Science Bulletin* **52**, 2780–8 (in Chinese with English abstract).
- Zhuang LL, Song YC, Liu YC, Fard M and Hou ZQ (2019) Major and trace elements and sulfur isotopes in two stages of sphalerite from the world-class Angouran Zn–Pb deposit, Iran: implications for mineralization conditions and type. *Ore Geology Reviews* **109**, 184–200.